

# FULLY GENERALIZED 2D CONSTRAINED DELAUNAY MESH REFINEMENT

PANAGIOTIS A. FOTEINOS\*, ANDREY N. CHERNIKOV†, AND NIKOS P. CHRISOCHOIDES‡

**Abstract.** Traditional refinement algorithms insert a Steiner point from a few possible choices at each step. Our algorithm, on the contrary, defines regions from where a Steiner point can be selected and thus inserts a Steiner point among an infinite number of choices. Our algorithm significantly extends existing generalized algorithms by increasing the number and the size of these regions. The lower bound for newly created angles can be arbitrarily close to 30 degrees. Both termination and good grading are guaranteed. It is the first Delaunay refinement algorithm with a 30 degree angle bound and with grading guarantees. Experimental evaluation of our algorithm corroborates the theory.

**Key words.** Delaunay triangulation, mesh generation

**AMS subject classifications.** 65D18, 68W05, 68W10, 68N19

**1. Introduction.** Delaunay refinement algorithms can be categorized into two families of algorithms: truly Delaunay and constrained Delaunay refinement algorithms. The former produce meshes which are truly Delaunay by repeatedly splitting the constrained segments until they appear in the mesh. The latter produce meshes which are as Delaunay as possible, i.e., they preserve most (but not all) of the nice properties of truly Delaunay triangulations [9, 20]. The advantage of constrained Delaunay refinement algorithms is that they produce meshes with fewer elements and guarantee better bounds on the minimum angles and grading. For these reasons, we chose to develop a constrained Delaunay refinement algorithm.

Traditional Delaunay refinement algorithms [8, 9, 13, 16, 19, 21] improve the quality of the mesh by inserting additional points into the mesh: the so-called *Steiner* points. Specifically, they insert the circumcenter of a bad triangle and the midpoint of an encroached segment.

There is no universal rule, however, for where the Steiner points should be inserted. In the literature, there are methods that insert points other than circumcenters and midpoints. For example, in [23], a bad triangle is split with its offcenter instead of its circumcenter producing a smaller mesh in practice. Similarly, in [11], a bad triangle is split by inserting a point chosen among a total number of four candidate points. Our goal is to develop an algorithm that allows for customizable point insertion strategies. This flexibility could also help to remove slivers in three dimensions deterministically, as opposed to randomized algorithms [10, 15]. In this paper, we show that there is an infinite number of Steiner points that can be chosen to split a triangle or a segment. The points that can be selected as Steiner points form *selection regions*. When a bad triangle is considered for splitting, the selection region is a two-dimensional region called *selection disk*. (Sometimes, we refer to selection disks as *selection circles*). Similarly, when a segment is considered for splitting, the

---

\*Department of Computer Science, College of William and Mary, Williamsburg, Virginia 23185 (pfot@cs.wm.edu).

†Department of Computer Science, College of William and Mary, Williamsburg, Virginia 23185 (ancher@cs.wm.edu).

‡Department of Computer Science, College of William and Mary, Williamsburg, Virginia 23185 (nikos@cs.wm.edu).

selection region is a one-dimensional region called *selection interval*.

Our group has already devised two generalized Delaunay refinement algorithms [5, 7]. The algorithm in [5] (called *Semi-Generalized Refinement* algorithm) deploys only selection disks, i.e., selection intervals are not used. Rather, each encroached segment is traditionally split at its midpoint. The algorithm in [7] (called *Generalized Refinement* algorithm) extends the Semi-Generalized Refinement algorithm by introducing the selection intervals. When the encroached segment to be split, however, forms an acute input angle, the selection interval is not defined; the Generalized Refinement algorithm traditionally splits such segments at their midpoint. In this paper, we extend the Generalized Refinement algorithm by introducing the selection interval of segments forming acute input angles.

Some of the applications of selection regions are discussed in our previous work. Specifically, our work in [4, 7] describes how the selection circles can be utilized in order to decrease the size of the mesh. In addition, our work in [6] shows how selection regions can incorporate many different point placement strategies performed in parallel.

As proved theoretically in [22] and shown practically in [12], mesh quality strongly affects the convergence speed and the solution accuracy of the finite element solver: the larger the minimum angle of the mesh is, the lower the condition number of the linear system becomes which yields a faster and a more robust solution.

Both the Semi-Generalized [5] and the Generalized Refinement algorithm [7] are proved to terminate with a lower angle bound as high as  $20.7^\circ$ . In this paper, we improve the quality of the mesh proving termination with a lower angle bound arbitrarily close (but not equal) to  $30^\circ$ .

Hudson [14] developed a theoretical framework for both two and three dimensions which shows that one can split elements at points other than their circumcenters. He, however, derives a rather weak angle bound in two dimensions: his algorithm guarantees that the lower bound for the angles is  $20.7^\circ$  (we guarantee that the lower bound for the angles is  $30^\circ$ ). Furthermore, his framework suffers from a severe restriction: the input cannot form acute angles. As it will become obvious in Section 3, the input of our algorithm can have acute angles as small as  $60^\circ$ .

To our knowledge, among the truly Delaunay refinement algorithms guaranteeing good grading, the algorithm presented by Miller, Pav, and Walkington [17] comes with the highest lower angle bound ( $26.45^\circ$ ). As far as constrained Delaunay refinement techniques are concerned, Chew [9] describes a constrained Delaunay refinement algorithm with a  $30^\circ$  lower angle bound, but with no proof of good grading. Shewchuk [21] shows that Chew's algorithm [9] offers good grading for a worse angle bound (i.e.,  $26.56^\circ$  instead of  $30^\circ$ ). In this paper, we show that Chew's algorithm produces well-graded elements with the original angle bound (i.e.,  $30^\circ$ ), confirming in this way the observations of practitioners. The work by Miller, Pav, and Walkington [17] does not address this issue; they focus on inputs with small input angles. In fact, the integration of our work in [17] is likely to yield graded elements with better angles near the boundary of the input.

In summary, the contributions of this paper are twofold:

- It extends the flexibility offered by the existing generalized algorithms [5, 7, 14]: our algorithm presented here increases the number and size of regions from where Steiner points can be chosen.
- It improves the guarantees on mesh quality: our algorithm terminates and produces well-graded triangles for a lower angle bound arbitrarily close to  $30^\circ$

degrees.

The rest of the paper is organized as follows. In Section 2, we shortly describe the traditional Delaunay refinement algorithms. In Section 3, we define the selection regions and give the pseudocode of our algorithm. In Section 4, we prove important lemmas and theorems needed for the proof of termination and good grading. The proof of good grading is presented in Section 5 and the proof of termination in Section 6. Finally, Section 7 experimentally evaluates our algorithm, and Section 8 concludes the paper.

**2. Delaunay Refinement Background.** The input domain  $\Omega$  to be meshed is usually described as a Planar Straight Line Graph (PSLG) [19, 21]. A PSLG  $\mathcal{X}$  is a set of input vertices and segments. The input segments are *constrained*, i.e., they have to appear in the final mesh, possibly as a union of smaller subsegments. We shall refer to an input segment as simply a *segment*. The input vertices should also be preserved in the final mesh. For brevity, we call both the segments and the input vertices *features*.

Let  $p_i, p_j$  be two vertices in the mesh. We denote the mesh edge that connects  $p_i$  with  $p_j$  as  $e(p_i, p_j)$  regardless of whether it is an input segment or not. The Euclidean distance between these points is denoted as  $\|p_i - p_j\|$ .

We use the circumradius-to-shortest-edge ratio  $\rho$  of a triangle to measure its quality. If the circumradius-to-shortest-edge ratio of a triangle  $t$  is equal to or larger than a specified upper bound  $\bar{\rho}$ , then  $t$  is said to be a poor or skinny triangle. Mesh refinement algorithms split poor triangles, until the circumradius-to-shortest-edge ratio of all the triangles in the mesh is less than  $\bar{\rho}$ . This upper bound sets a lower bound for the angles in the mesh, since the circumradius-to-shortest-edge ratio of a triangle with shortest edge  $l$ , circumradius  $r$ , and smallest angle  $A$  is  $\rho = \frac{r}{l} = \frac{1}{2\sin A}$  [18, 21]. Therefore, when the refinement terminates, it is guaranteed that all the angles in the mesh are larger than  $\arcsin \frac{1}{2\bar{\rho}}$ . For brevity, we denote this angle lower bound as  $\theta$ :  $\theta = \arcsin \frac{1}{2\bar{\rho}}$ . Clearly,  $\theta$  can only be an acute angle.

A triangle  $t$  is said to satisfy the *constrained Delaunay property*, if there is no vertex that lies strictly inside  $t$ 's circumscribed circle (*circumcircle*) and is visible from the interior of  $t$  [9, 21]. Two vertices  $p_i, p_j$  are visible to each other, if the line connecting  $p_i$  with  $p_j$  does not intersect (at exactly one point) the interior of any constrained segment. See Figure 2.1(left) and Figure 2.1(middle). At any time during the refinement process, all the triangles in the mesh have to satisfy the constrained Delaunay property.

*Cavity* [13] of a point  $p$  is defined to be the set  $\mathcal{C}(p)$  of triangles  $t_i$  in the mesh, such that the circumcircle of every  $t_i$  in  $\mathcal{C}(p)$  includes the point  $p$ , and  $p$  is visible from the interior of  $t_i$  (see Figure 2.1(right)). We denote  $\partial\mathcal{C}(p)$  to be the set of boundary edges of the cavity, i.e., the edges which are incident upon only one triangle in  $\mathcal{C}(p)$ . For our analysis, we use the Bowyer-Watson (B-W) point insertion algorithm [3, 24], which can be written shortly as in Algorithm 1. Note that this definition of a cavity implies that if  $p$  is inserted into the mesh, then all the triangles in  $\mathcal{C}(p)$  do not satisfy the constrained Delaunay property and must be deleted. After the deletion of these triangles, the cavity has to be re-triangulated, such that all the newly formed triangles respect the constrained Delaunay property.

As mentioned above, refinement algorithms repeatedly split skinny triangles, until the ratio of all the triangles in the mesh is less than the upper bound  $\bar{\rho}$ . Traditionally, a skinny triangle  $t$  is deleted by inserting its circumcenter  $p$  (using the Bower-Watson point insertion algorithm). We will show, however, that there is a

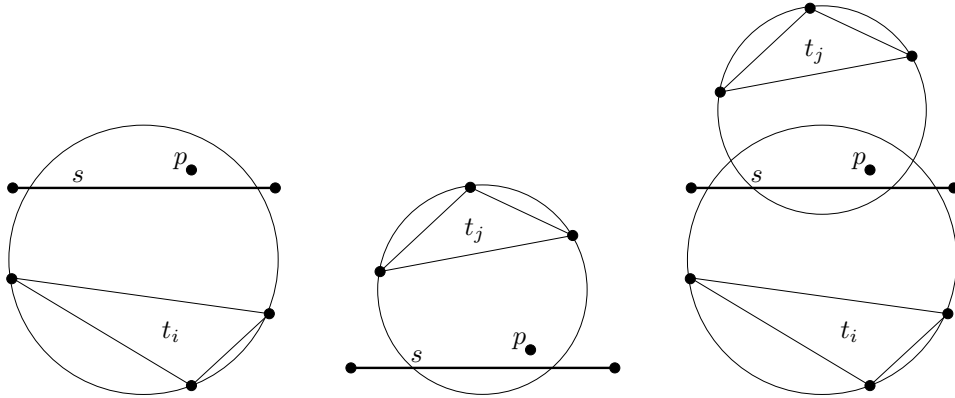


FIG. 2.1. **(Left)** Triangle  $t_i$  satisfies the constrained Delaunay property: although  $p$  is inside the circumcircle, it is not visible from the interior of  $t_i$  because of the constrained segment  $s$ . **(Middle)** Triangle  $t_j$  does not respect the constrained Delaunay property:  $p$  lies inside the circumcircle and is visible from the interior of  $t_j$ . **(Right)** The cavity  $\mathcal{C}(p)$  of  $p$  includes only the triangle  $t_j$ . Although  $p$  lies inside  $t_i$ 's circumcircle,  $t_i$  does not belong to  $\mathcal{C}(p)$ , since  $p$  is not visible from the interior of  $t_i$ . Notice that  $t_i$  respects the constrained Delaunay property, but  $t_j$  does not; therefore,  $t_j$  must be deleted.

---

**Algorithm 1:** The Bowyer-Watson point insertion procedure.

---

1 **Algorithm:**  $\text{BowyerWatson}(V, T, p)$

**Input** :  $V$  is the set of vertices.  
 $T$  is the set of triangles.  
 $p$  is the Steiner point to be inserted.

**Output:**  $V$  and  $T$  after the insertion of  $p$ .

2  $V \leftarrow V \cup \{p\};$   
3  $T \leftarrow T \setminus \mathcal{C}(p) \cup \{(p\xi) \mid \xi \in \partial\mathcal{C}(p)\};$

---

whole two-dimensional space inside the circumcircle of  $t$  where a Steiner point  $p$  can be chosen from.

Even though the Steiner point  $p$  of a skinny triangle  $t_i$  is always inserted inside  $t_i$ 's circumcircle,  $t_i$  may not belong to  $\mathcal{C}(p)$ . This can happen when  $p$  is not visible from the interior of  $t_i$ ; that is, when  $t_i$  and  $p$  lie on opposite sides of a constrained segment. See Figure 2.1(right) for an illustration: in such a case, the insertion of  $p$  fails to remove the skinny triangle  $t_i$  from the mesh. To deal with these circumstances and to prevent the insertion of Steiner points outside the domain, Delaunay refinement algorithms obey special *encroachment* rules [9, 21]. We define encroachment as follows:

DEFINITION 2.1. (*Encroachment of a constrained segment*) A segment  $s$  is said to be encroached upon by a skinny triangle  $t$ , if  $p_i$  is not visible from the interior of  $t$  due to  $s$ , i.e., the line connecting  $p_i$  and any point in the interior of  $t$  intersects the interior of  $s$ . If more than one segment lies between  $t$  and  $p_i$ , encroached is the segment closest to  $t$ .

See Figure 2.2 for an illustration.

If a skinny triangle  $t$  encroaches upon a segment  $s$ , then its Steiner point is rejected from the mesh. In addition, all the *free* vertices (i.e., vertices that neither are input vertices nor lie on segments) which lie inside the diametral circle of  $s$  and are visible

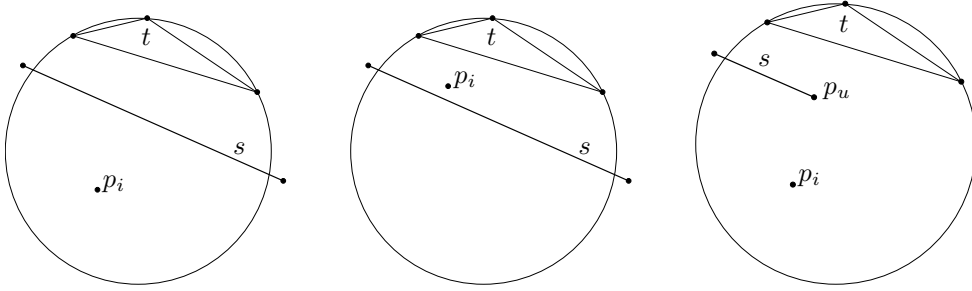


FIG. 2.2. A skinny triangle  $t$  and its Steiner point  $p_i$  when **(Left)**  $t$  encroaches upon segment  $s$ , and when **(Middle)** it does not. **(Right)** Does  $t$  encroach upon  $s$  or not? No matter where  $p_i$  is, this case illustrated in this subfigure cannot happen, since  $t$  did not satisfy the constrained Delaunay property before the insertion of  $p_i$ . Indeed,  $p_u$  lies inside  $t$ 's circumcircle and is visible from the interior of  $t$ , because the line connecting  $p_u$  with any point in the interior of  $t$  does not intersect the interior of  $s$  but one of its endpoints.

from the interior of  $s$  are deleted. (The diametral circle of a segment is the circle with diameter that segment.) Then, a new Steiner point is inserted on  $s$ . Traditionally, the midpoint of  $s$  is inserted, but we will show that there is a whole one-dimensional space inside  $s$  where a Steiner point can be chosen from.

The following definitions of the *local feature size*, *insertion radius*, and *parent* play a central role in the analysis in [19, 21], and we use them for our analysis in the generalized form, too.

DEFINITION 2.2 (Local feature size [19, 21]). *The local feature size function  $\text{lfs}(p)$  for a given point  $p$  is equal to the radius of the smallest disk centered at  $p$  that intersects two non-incident features of the PSLG.*

$\text{lfs}(p)$  satisfies the Lipschitz condition:

LEMMA 2.3 (Lemma 1 in [19], Lemma 2 in [21]). *Given any PSLG and any two points  $p_i$  and  $p_j$ , the following inequality holds:*

$$\text{lfs}(p_i) \leq \text{lfs}(p_j) + \|p_i - p_j\|. \quad (2.1)$$

DEFINITION 2.4 (Insertion radius). *The insertion radius  $R(p)$  of point  $p$  is the distance from  $p$  to its nearest visible vertex, immediately after  $p$  is inserted. If  $p$  is an input vertex, then  $R(p)$  is the Euclidean distance between  $p$  and the nearest input vertex visible from  $p$ .*

REMARK 1. *Assume that  $p_l$  and  $p_m$  are mutually visible vertices inserted into the mesh, and that  $p_l$  was inserted after  $p_m$  (or both  $p_l$  and  $p_m$  are input vertices), then  $R(p_l) \leq \|p_l - p_m\|$ . Indeed, if  $p_m$  was the closest visible vertex from  $p_l$  at the time  $p_l$  was inserted into the mesh (in the case of input vertices, assume that they were inserted simultaneously), then  $R(p_l) = \|p_l - p_m\|$  by the definition of the insertion radius; otherwise,  $R(p_l) < \|p_l - p_m\|$ .*

REMARK 2. *As shown in [21], if  $p$  is an input vertex, then  $R(p) \geq \text{lfs}(p)$ . Indeed, the (closed) disk with center  $p$  and radius  $R(p)$  intersects two non-incident features: the input vertex  $p$  and  $p$ 's closest visible vertex.*

Below, we define the parent of a Steiner point:

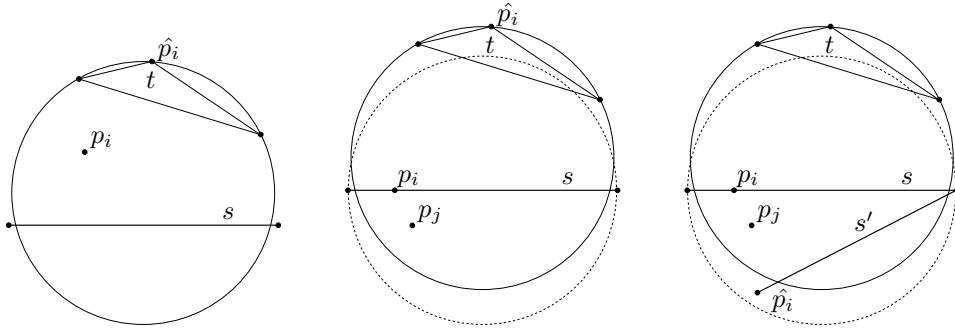


FIG. 2.3. Different cases of parenthood as defined in Definition 2.5.  $t$  is a skinny triangle,  $p_i, p_j$  are Steiner points, and  $s, s'$  are (constrained) segments. Point  $p_i$  is inserted after  $p_j$ . **(Left)**  $t$  does not encroach upon  $s$ , and therefore its Steiner point  $p_i$  is not rejected. The parent  $\hat{p}_i$  of  $p_i$  is the most recently inserted vertex of  $t$ 's shortest edge. **(Middle)**  $t$  encroaches upon  $s$  and its Steiner point  $p_j$  is rejected. Instead, the Steiner point  $p_i$  is inserted on  $s$ . Since the diametral circle of  $s$  is empty of non-free vertices, the parent of  $p_i$  is the most recently inserted vertex of  $t$ 's shortest edge. **(Right)**  $t$  encroaches upon  $s$ , and therefore its Steiner point  $p_j$  is rejected. Instead, the Steiner point  $p_i$  is inserted on  $s$ . Since the diametral circle of  $s$  contains a non-free vertex, lying on the constrained segment  $s'$ , the parent  $\hat{p}_i$  of  $p_i$  is this non-free vertex.

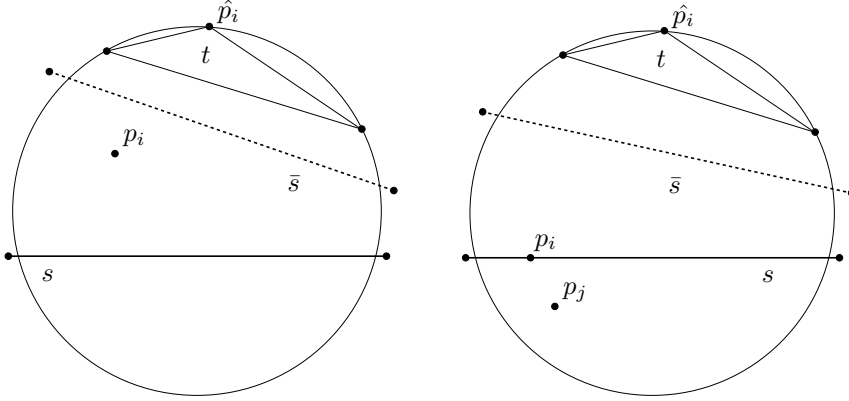


FIG. 2.4. The constrained segment  $\bar{s}$  is shown with the dashed line. **(Left)** Rule-2 applies (i.e.,  $p_i$  is not rejected), as in Figure 2.3(left), but now  $\bar{s}$  obstructs visibility between  $p_i$  and  $\hat{p}_i$ . **(Right)** Rule-3 applies (i.e.,  $t$  encroaches upon  $s$ ), as in Figure 2.3(middle), but now  $\bar{s}$  obstructs visibility between  $p_i$  and  $\hat{p}_i$ .

DEFINITION 2.5 (Parent of a Steiner point). The parent  $\hat{p}_i$  of point  $p_i$  is the vertex defined by the following four rules:

- Rule-1.** If  $p_i$  is either an input vertex or a rejected vertex, then it has no parent.
- Rule-2.** If  $p_i$  is inserted inside the circumcircle of a poor quality triangle  $t$ ,  $\hat{p}_i$  is the most recently inserted vertex of the shortest edge of  $t$ . See Figure 2.3(left).
- Rule-3.** If  $p_i$  is inserted on a segment  $s$ , encroached upon by a skinny triangle  $t$ , and no non-free vertex visible from  $p_i$  lies inside the diametral circle of  $s$ , then  $\hat{p}_i$  is the most recently inserted vertex of the shortest edge of the encroaching triangle. See Figure 2.3(middle).
- Rule-4.** If  $p_i$  is inserted on a segment  $s$ , encroached upon by a skinny triangle  $t$ , and at least one non-free vertex visible from  $p_i$  lies inside the diametral circle of  $s$ , then  $\hat{p}_i$  is the closest-to- $p_i$  such a non-free vertex. See Figure 2.3(right).

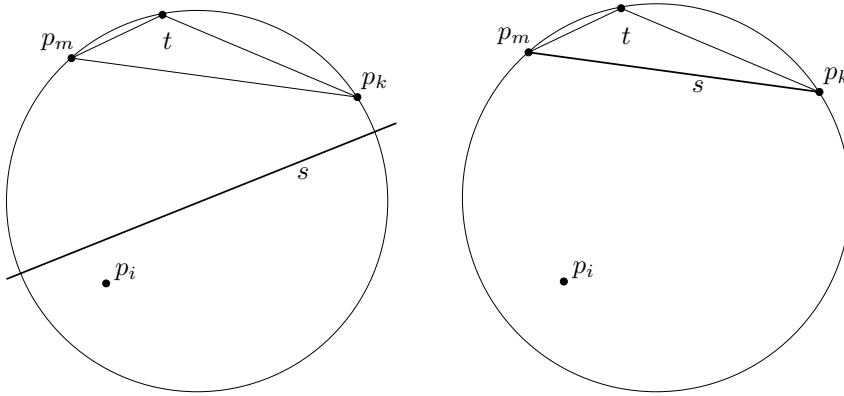


FIG. 2.5. The separator of an encroached (constrained) segment  $s$ . A skinny triangle  $t$  encroaches upon the constrained segment  $s$  (because  $t$  and its Steiner point  $p_i$  lie on opposite sides of  $s$ ). The edge  $e(p_m p_k)$  is the separator of  $s$ . Intuitively, the separator of  $s$  is the edge of  $t$  which  $s$  would fall on, if we moved  $s$  towards  $t$ . The right figure illustrates the special case where the encroached segment coincides with its separator.

LEMMA 2.6. The parent  $\hat{p}_i$  (if one exists) of a point  $p_i$  is visible from  $p_i$ .

*Proof.* Let  $p_i$  be a vertex and  $\hat{p}_i$  be its parent. For the sake of contradiction, assume that  $\hat{p}_i$  is not visible from  $p_i$  due to a segment  $\bar{s}$ , i.e., the line connecting  $p_i$  and  $\hat{p}_i$  intersects the interior of  $\bar{s}$ . We will investigate what that means for each rule of Definition 2.5.

Rule-1 does not apply, since we have assumed that  $p_i$  does have a parent in this lemma. This also implies that  $p_i$  is neither an input nor a rejected vertex.

If Rule-2 applies, then consider Figure 2.4(left): the skinny triangle  $t$  must encroach upon  $\bar{s}$ . But that means that  $p_i$  should have been rejected from the mesh: a contradiction.

If Rule-3 applies, then consider Figure 2.4(right): the skinny triangle  $t$  does not encroach upon  $s$  but upon  $\bar{s}$ : a contradiction.

Finally, if Rule-4 applies,  $\hat{p}_i$  and  $p_i$  are visible to each other by definition: a contradiction.  $\square$

Notice that a rejected point does not have a parent according to our definition (Rule-1), while it does in the traditional approaches. This change is not necessary, but it considerably simplifies the proofs in the next sections.

Also, observe that the parent of a Steiner point  $p_i$  inserted on an encroached, constrained segment  $s$  might lie outside the diametral circle of  $s$  (see Figure 2.3(middle) for an illustration). This is different from the traditional approaches where the parent of  $p_i$  is always inside or on the diametral circle of the encroached segment. This modification of the parent definition is crucial, since the diametral circle of an encroached segment might not contain any traditional parent candidates at all in our generalized algorithm. For our analysis, it is useful to know whether the parent of  $p_i$  is strictly inside the diametral circle of  $s$  or not; we, therefore, classify the parent as either an *external* or a *non-external* parent according to the following definition:

DEFINITION 2.7 (External parent). Assume that  $p_i$  is a Steiner point inserted on an encroached segment  $s$ . If its parent  $\hat{p}_i$  lies on or outside the diametral circle of  $s$ , then we say that  $\hat{p}_i$  is an external parent. Conversely, if  $\hat{p}_i$  lies strictly inside the diametral circle of  $s$ , then we say that  $\hat{p}_i$  is a non-external parent.

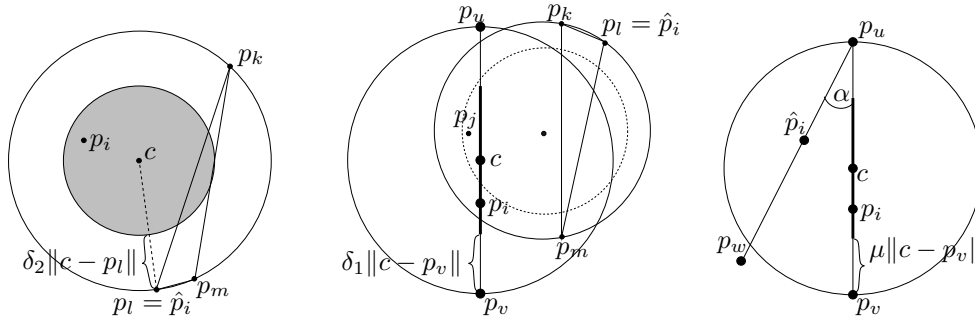


FIG. 3.1. The three kinds of selection regions. Big dots denote non-free vertices lying on (constrained) segments, while small dots denote free vertices. Point  $c$  is not a part of the mesh; it is rather an auxiliary point that denotes the center of the selection regions. Point  $p_i$  is a Steiner point inserted into the mesh. Point  $p_j$  is a Steiner point rejected from the mesh. **(Left)** Selection circle (shaded) for the skinny triangle  $\Delta p_k p_l p_m$  with the shortest edge  $e(p_l p_m)$ . Also illustrates case (1) from Table 4.1. **(Middle)** Type-B selection interval (bold) for an encroached segment  $e(p_u p_v)$ . Also illustrates case (2) from Table 4.1. The constrained segment  $e(p_u p_v)$  is encroached since the skinny triangle  $\Delta p_k p_l p_m$  and its Steiner point  $p_j$  lie on opposite sides. The Steiner point  $p_j$  is rejected, and the diametral circle is emptied of vertices which are free and visible from the interior of  $e(p_u p_v)$ ; in this example, only the free vertex  $p_m$  is deleted. Another Steiner point  $p_i$  in the Type-B selection interval of  $e(p_u p_v)$  is inserted instead. The parent  $\hat{p}_i$  of the vertex  $p_i$  may be an external vertex (as depicted), i.e., a vertex outside the diametral circle of  $e(p_u p_v)$ . **(Right)** Type-C selection interval (bold) for an encroached segment  $e(p_u p_v)$ . Also illustrates case (4) from Table 4.1. The Steiner point  $p_i$  has been inserted in the Type-C selection interval. The parent  $\hat{p}_i$  is a non-external vertex which lies on a segment incident to  $e(p_u p_v)$ . The input angle formed by the segments  $e(p_u p_v), e(p_u p_w)$  is denoted with  $\alpha$ .

For example, the point  $\hat{p}_i$  is an external parent in Figure 2.3(middle), but it is a non-external parent in Figure 2.3(right).

REMARK 3. If  $p$  is inserted on a segment  $s$  encroached upon by a skinny triangle  $t$ , and  $\hat{p}$  is an external parent, then  $\hat{p}$  is the most recently inserted vertex of  $t$ 's shortest edge. Indeed, if Rule-3 did not apply, then Rule-4 would, i.e.,  $\hat{p}$  would lie inside the diametral circle of  $s$ : a contradiction.

Next, we define the *separator* of an encroached segment:

DEFINITION 2.8 (Separator of an encroached, constrained segment). Let  $t$  encroach upon a segment  $s$ . The separator of  $s$  is the unique edge of  $t$  that lies between  $s$  and the interior of  $t$ .

Notice that the separator of an encroached segment always exists and is unique. See Figure 2.5 for a couple of examples.

The density [21] of a vertex  $p$ , denoted as  $D(p)$ , is defined as:

$$D(p) = \frac{\text{lfs}(p)}{R(p)}. \quad (2.2)$$

Refinement algorithms are proved to produce well-graded triangles by showing that the density of all mesh vertices is less than a constant.

**3. Generalized Delaunay Refinement Algorithm.** In the following sections, we will show that our Generalized Constrained Delaunay Refinement (GCDR) algorithm guarantees termination and good grading for a circumradius-to-shortest-edge ratio upper bound  $\bar{\rho}$  arbitrarily close to 1. This value for  $\bar{\rho}$  corresponds to an angle lower bound of  $\theta = \arcsin \frac{1}{2} = 30$  degrees.



DEFINITION 3.1 (Selection circle). For a skinny triangle with circumcenter  $c$ , shortest edge length  $l$ , circumradius  $r$ , and circumradius-to-shortest-edge ratio  $\rho = r/l \geq \bar{\rho} \geq 1$ , the selection circle is the circle with center  $c$  and radius  $r(1 - \delta_2)$ , where  $\delta_2$  is a constant parameter chosen such that

$$\frac{1}{\bar{\rho}} \leq \delta_2 \leq 1. \quad (3.1)$$

See Figure 3.1(left) for an illustration.

REMARK 4. If  $\delta_2 = 1$ , then the selection circle shrinks to the circumcenter point.

DEFINITION 3.2 (Type-B selection interval). If  $s$  is an encroached segment with center  $c$ , then the Type-B selection interval of  $s$  is the subsegment of  $s$  with center  $c$  and length  $|s|(1 - \delta_1)$ , where  $\delta_1$  is a constant parameter chosen such that

$$\frac{1}{\bar{\rho}\delta_2} \leq \delta_1 \leq 1, \quad (3.2)$$

and  $|s|$  is the length of  $s$ . See Figure 3.1(middle) for an illustration.

REMARK 5. If  $\delta_1 = 1$ , then the Type-B selection interval shrinks to the center point.

REMARK 6. If  $\bar{\rho} = 1$ , then both  $\delta_2$  and  $\delta_1$  can only be equal to 1; therefore, both the selection circles of skinny triangles and the Type-B selection intervals of encroached segments shrink to the respective center points.

REMARK 7. If  $\delta_2 = \frac{1}{\bar{\rho}}$ , then  $\delta_1$  can only be equal to 1; therefore, the Type-B selection intervals of encroached segments shrink to the center points.

REMARK 8. If  $\delta_1 = \frac{1}{\bar{\rho}}$ , then  $\delta_2$  can only be equal to 1; therefore, the selection circles shrink to the circumcenters.

DEFINITION 3.3 (Type-C selection interval). If  $s$  is a segment with center  $c$ , then the Type-C selection interval of  $s$  is the subsegment of  $s$  with center  $c$  and length  $|s|(1 - \mu)$ , where  $\mu$  is a constant parameter chosen such that

$$2 \cos \alpha_{\min} \leq \mu \leq 1, \quad (3.3)$$

and  $\alpha_{\min}$  is the minimum input angle in the PSLG. Clearly,  $\alpha_{\min}$  cannot be smaller than  $60^\circ$ . See Figure 3.1(right) for an illustration.

REMARK 9. If  $\mu = 1$ , then the Type-C selection interval shrinks to the center point. In our previous Generalized algorithms [5, 7], the Type-C selection interval is always the center point.

REMARK 10. If  $\alpha_{\min}$  is equal to  $60^\circ$ , then  $\mu$  can only be equal to 1, and therefore the Type-C selection interval of the corresponding segment shrinks to its center point.

REMARK 11. If  $\delta_1 = \delta_2 = \mu = 1$ , then our GCDR algorithm is identical to Chew's second algorithm, as described in [21].

Algorithm 2 presents the GCDR algorithm. For brevity, let us classify the non-rejected Steiner points, inserted by the GCDR algorithm, into three categories:

---

**Algorithm 2:** The Generalized Constrained Delaunay Refinement algorithm.

---

1 **Algorithm:** GeneralizedDelaunayRefinement( $\mathcal{X}$ ,  $\bar{\rho}$ ,  $\delta_2$ ,  $\delta_1$ ,  $\mu$ ,  $F_A()$ ,  $F_B()$ ,  $F_C()$ ,  $\mathcal{M}$ )

**Input** :  $\mathcal{X}$  is the input PSLG.

$\bar{\rho}$  is the upper bound on circumradius-to-shortest-edge ratio,  $\bar{\rho} \geq 1$ .

$\delta_2$  is the parameter which defines selection circles for skinny triangles,  $\frac{1}{\bar{\rho}} \leq \delta_2 \leq 1$ .

$\delta_1$  is the parameter which defines Type-B selection intervals of encroached segments,  $\frac{1}{\bar{\rho}\delta_2} \leq \delta_1 \leq 1$ .

$\mu$  is the parameter which defines Type-C selection intervals of encroached segments,  $2 \cos \alpha_{\min} \leq \mu \leq 1$ , where  $\alpha_{\min}$  is the minimum input angle present in  $\mathcal{X}$ .

$F_A()$ ,  $F_B()$ , and  $F_C()$  are user-defined functions which return specific Steiner points within selection circles and selection intervals, respectively.

$\mathcal{M} = (V, T)$  is an initial constrained Delaunay triangulation of  $\mathcal{X}$ , where  $V$  is the set of vertices and  $T$  is the set of triangles.

**Output:** A constrained Delaunay mesh  $\mathcal{M}$  whose triangles have circumradius-to-shortest-edge ratio less than  $\bar{\rho}$ .

```

2 Let SkinnyTriangles be the set of triangles in  $T$  whose
  circumradius-to-shortest-edge ratio is larger than or equal to  $\bar{\rho}$ ;
3 while SkinnyTriangles  $\neq \emptyset$  do
4   Pick  $t \in$  SkinnyTriangles;
5    $p \leftarrow F_A(\mathcal{M}, \delta_2, t)$ ;           /*  $p$  is of Type-A */
6   if  $t$  encroaches upon a segment  $s$  then   /*  $p$  is rejected */
7     Delete the free vertices inside the diametral circle of  $s$ ;
8     if there is a non-free vertex which lies strictly inside the diametral
       circle of  $s$  and is visible from the interior of  $s$  then
9        $p \leftarrow F_C(\mathcal{M}, \mu, s)$ ;       /*  $p$  is of Type-C */
10    else
11       $p \leftarrow F_B(\mathcal{M}, \delta_1, s)$ ;   /*  $p$  is of Type-B */
12    end
13  end
14  BowyerWatson( $V, T, p$ ) ;           /* insert  $p$  into the mesh */
15  Update SkinnyTriangles;
16 end

```

---

- If a point  $p_i$  is inserted inside the selection circle of skinny triangle, then  $p_i$  is called a *Type-A* point.
- If a point  $p_i$  is inserted on an encroached segment  $s$ , and there is no non-free vertex strictly inside the diametral circle of  $s$  and visible from  $p_i$ , then  $p_i$  is called a *Type-B* point. Type-B points are only inserted in the Type-B selection interval of encroached segments.
- If a point  $p_i$  is inserted on an encroached segment  $s$ , and there is at least one non-free vertex strictly inside the diametral circle of  $s$  and visible from  $p_i$ , then  $p_i$  is called a *Type-C* point. Type-C points are only inserted in the Type-C selection interval of encroached segments.

For example, the vertex  $p_i$  in Figure 3.1(left), Figure 3.1(middle), and Figure 3.1(right) is a Type-A, Type-B, and a Type-C point respectively.

Notice that the parent of Type-B and Type-C points is not the same as in our previous Generalized Refinement algorithm presented in [7]: the parent  $\hat{p}$  of a Type-C point  $p$  is now a non-free vertex strictly inside the diametral circle of an encroached segment  $s$ , regardless of whether  $\hat{p}$  lies on a segment incident to  $s$  or not. This change is not necessary, but it further simplifies the proofs of the sections followed.

The analysis below assumes that all angles in the input PSLG are not less than  $60^\circ$ . (Input angles less than 60 degrees can be removed via postprocessing techniques [9] or via concentric circular shell splitting [19, 21], but without guarantee of good grading.)

**4. Point Spacing Theorem.** The main result of this section is Theorem 4.6 which establishes the relation between the insertion radius of a point and that of its parent or the local feature size. In particular, in both cases, the insertion radius is bounded from below and, therefore, the lengths of the edges created by the GCDR algorithm are bounded from below. This result allows us to prove in the following sections the termination of the algorithm and the good grading of the meshes it produces.

First, we prove Lemmas 4.1, 4.2, 4.3, 4.4, and 4.5 that establish important relations used in the proof of Theorem 4.6 as well as in the proof of good grading in Section 5. Lemmas 4.1, 4.2, and 4.3 bound the insertion radius of a Steiner point from below in terms of the size of the two-dimensional and one-dimensional selection region, respectively. Lemma 4.4 relates the length of the encroached segment with the length of the circumradius of the encroaching triangle. Finally, Lemma 4.5 determines which of the edges of a skinny triangle can be the shortest.

LEMMA 4.1. *If a Steiner point  $p_i$  is of Type-A, then*

$$R(p_i) \geq \delta_2 r, \quad (4.1)$$

where  $r$  is the circumradius of the corresponding skinny triangle.

*Proof.* Consider Figure 3.1(left). By the way we defined Type-A Steiner points (see section 3),  $p_i$  is actually inserted into the mesh; therefore, there is no segment that lies between  $p_i$  and the skinny triangle  $t = \triangle p_k p_l p_m$  (i.e.,  $t$  does not encroach upon any segment). By the constrained Delaunay property,  $t$ 's circumcircle does not contain vertices visible from  $t$ 's interior. Since  $p_i$  and  $t$  lie on the same side of any constrained segment, there is no vertex inside the circumcircle which is visible from  $p_i$ . Therefore, the donut between the boundary of the circumcircle and the boundary of the selection circle cannot contain points visible from  $p_i$ . Thus, the distance from  $p_i$  to the closest mesh vertex visible from  $p_i$  has to be greater than or equal to the width of the donut. This implies that the insertion radius of  $p_i$  has to be greater than or equal to the width of the donut which is equal to  $\delta_2 r$ .  $\square$

LEMMA 4.2. *If a Steiner point  $p_i$ , inserted on an encroached segment  $s$ , is of Type-B, and  $\hat{p}_i$  is either a Type-A point or a non-free external parent, then*

- *there are no non-free vertices inside the diametral circle of  $s$  that are visible from  $p_i$ , and*
- *the following inequality holds:*

$$R(p_i) \geq \delta_1 \frac{|s|}{2}. \quad (4.2)$$

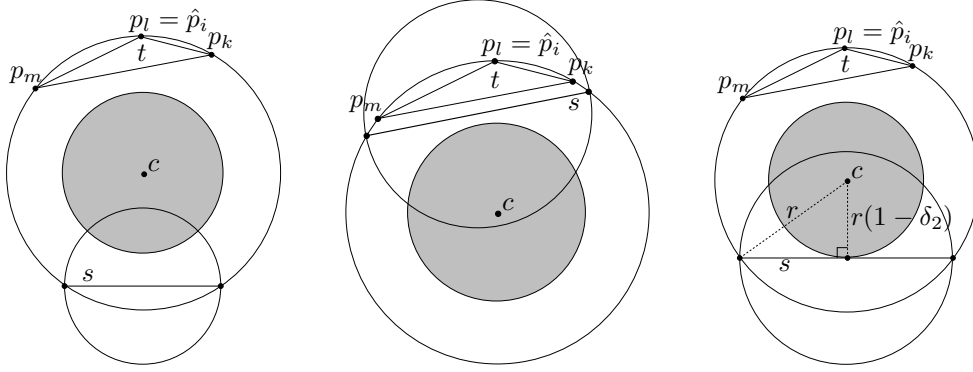


FIG. 4.1. The shaded circle represents the selection circle of the skinny triangle  $t$ . Point  $c$  is the center of the selection circles. **(Left)** Segment  $s$  does not intersect the selection circle, but  $t$  cannot encroach upon  $s$ . **(Middle)** Segment  $s$  does not intersect the selection circle,  $t$  encroaches upon  $s$ , but  $\hat{p}_i$  is not an external parent, since it lies strictly inside the diametral circle of  $s$ . **(Right)** If  $s$  intersects the selection circle, then its length is minimized when it is tangent to the selection circle. The radius of  $t$ 's circumcircle is denoted as  $r$ .

*Proof.* For the first part, for the sake of contradiction, assume that the diametral circle of  $s$  is not empty of non-free vertices visible from  $p_i$ . Let  $p_j$  be the closest-to- $p_i$ , non-free vertex which is inside the diametral circle of  $s$  and visible from  $p_i$ . By Definition 2.5 (Rule-4),  $p_j$  is the parent of  $p_i$ . However,  $p_j$  is neither a Type-A point (since it is a non-free vertex) nor an external parent (since it lies inside the diametral circle of  $s$ ): a contradiction.

For the second part, recall that all the free vertices which are inside the diametral circle of  $s = e(p_u p_v)$  (see Figure 3.1(middle)) and visible from the interior of  $s$  are deleted. Also, from the first part above, there are no non-free vertices which lie inside the diametral circle of  $s$  and are visible from  $p_i$ . Therefore, one of the endpoints of  $s$  — say the endpoint  $p_v$  — is the vertex closest to  $p_i$  among the vertices that are visible from  $p_i$ . This means that  $R(p_i) = \|p_i - p_v\|$ , and from the definition of the Type-B selection interval,  $R(p_i) \geq \delta_1 \frac{|s|}{2}$ .  $\square$

LEMMA 4.3. If  $p_i$ , inserted on an encroached segment  $s$ , is of Type-C, then

- if  $\hat{p}_i$  is the closest vertex to  $p_i$ , the following equality holds:

$$R(p_i) = \|p_i - \hat{p}_i\|, \quad (4.3)$$

or

- if one of the endpoints of  $s$  is closest to  $p_i$ , the following inequality holds:

$$R(p_i) \geq \mu \frac{|s|}{2}. \quad (4.4)$$

*Proof.* Consider Figure 3.1(right). By the way we defined a Type-C point, there is at least one non-free vertex strictly inside the diametral circle of  $s = e(p_u p_v)$  and visible from the interior of  $s$  (i.e., visible from  $p_i$ ). Therefore, by Definition 2.5 (Rule-4),  $\hat{p}_i$  is the closest-to- $p_i$ , non-free vertex visible from the interior of  $s$ . Recall, however, that all the free vertices which are inside the diametral circle of  $s$  and visible from the interior of  $s$  are deleted. Therefore, there are two scenarios: either  $\hat{p}_i$  or one of the endpoints of  $s$  is the closest vertex to  $p_i$ . In the first case, equation (4.3) holds

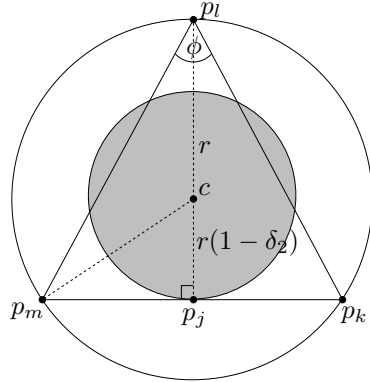


FIG. 4.2. The skinny triangle  $t = \Delta p_k p_l p_m$  where  $e(p_m p_k)$  is the separator of the encroached segment. Since  $e(p_m p_k)$  is tangent to the selection circle at the point  $p_j$ , angle  $\phi$  takes its minimum value. Without loss of generality,  $t$  is an isosceles triangle with  $e(p_m p_k)$  being the base.

by definition of the insertion radius (Definition 2.4). In the second case, since  $p_i$  is inserted in the Type-C selection interval of  $s$ ,  $p_i$  is separated from the endpoints of  $s$  by a distance at least  $\mu \frac{|s|}{2}$ , and inequality (4.4) holds.  $\square$

LEMMA 4.4. Let  $p_i$  be a Steiner point inserted on a segment  $s$  encroached upon by a skinny triangle  $t$  with circumradius equal to  $r$ . If the parent of  $p_i$  is an external parent, then

- $s$  intersects  $t$ 's selection circle, and
- the following inequality holds:

$$\frac{|s|}{2} \geq r \sqrt{2\delta_2 - \delta_2^2}. \quad (4.5)$$

*Proof.* From Remark 3, we obtain that the parent  $\hat{p}_i$  of  $p_i$  is a vertex of  $t$  (in fact,  $\hat{p}_i$  is the most recently inserted vertex of  $t$ 's shortest edge). We claim that  $s$  has to intersect  $t$ 's selection circle. Indeed, if it does not, either  $s$  cannot be encroached upon by  $t$  (see Figure 4.1(left)), or  $p_i$  cannot be an external parent (see Figure 4.1(middle)): a contradiction.

For the second part, observe that the length of  $s$  reaches its smallest value when  $s$  is tangent to  $t$ 's selection circle, and its endpoints lie precisely on  $t$ 's circumcircle. See Figure 4.1(right) for an illustration. From the right triangle formed, we obtain that  $\frac{|s|}{2}$  is at least  $\sqrt{r^2 - r^2(1 - \delta_2)^2}$ , and equation (4.5) holds.  $\square$

LEMMA 4.5. Let triangle  $t$  encroach upon the constrained segment  $s$ . The separator of  $s$  cannot be the shortest edge of  $t$ .

*Proof.* See Figure 3.1(middle). From Definition 2.8, the separator of  $s = e(p_u p_v)$  is the edge  $e(p_m p_k)$ . We will prove the Lemma by showing that the angle  $\angle p_k p_l p_m$  cannot be the smallest angle of the encroaching triangle  $t = \Delta p_k p_l p_m$ .

For the sake of contradiction, assume that  $\phi = \angle p_k p_l p_m$  is the smallest angle of  $t$ . It is well-known that all inscribed angles subtended by the same arc of a circle are equal. Therefore, we can turn  $t$  into an isosceles triangle, without changing the value of  $\phi$ , by moving appropriately the point  $p_l$  on  $t$ 's circumcircle. Now, observe that the value of  $\phi$  decreases as the endpoints of  $e(p_m p_k)$  move on  $t$ 's circumcircle and

		$\hat{p}_i$						
		Type-A	Type-B			Type-C or input		
$p_i$	Type-A	(1)						
	Type-B	(2)	(3)	n/a	n/a	(3)	n/a	n/a
	Type-C	n/a	n/a	(4)	(5)	n/a	(4)	(5)
		external	incident	non-incident			incident	non-incident
			non-external		external	non-external		

TABLE 4.1

All possible type combinations of  $p_i$  and  $\hat{p}_i$ . The cells above labels “external” and “non-external” correspond to the cases when  $\hat{p}_i$  is an external and a non-external parent respectively. Also, the cells above labels “incident” and “non-incident” correspond to the cases when  $p_i$  and  $\hat{p}_i$  lie on incident and non-incident constrained segments respectively. Each of the cases (n) is analyzed separately.

away from the point  $p_l$ . Thus, the smallest value that  $\phi$  can take is when  $e(p_m p_k)$  is tangent to the selection circle of  $t$ , as depicted in Figure 4.2. Note that the edge  $e(p_m p_k)$  cannot move further away from  $p_l$ , since otherwise  $t$  could not encroach upon  $s$  any more.

See Figure 4.2. From the right triangle  $\triangle p_m p_j c$ , we obtain that  $\|p_m - p_j\| = r\sqrt{\delta_2(2 - \delta_2)}$ . Similarly, from the right triangle  $\triangle p_m p_j p_l$ , we obtain that  $\|p_m - p_l\| = r\sqrt{2(2 - \delta_2)}$ . Therefore, we have that

$$\begin{aligned}
\sin \frac{\phi}{2} &= \frac{\|p_m - p_j\|}{\|p_m - p_l\|} && \text{(from the right triangle } \triangle p_m p_j p_l) \\
&= \frac{r\sqrt{\delta_2(2 - \delta_2)}}{r\sqrt{2(2 - \delta_2)}} \\
&= \sqrt{\frac{\delta_2}{2}} \\
&\geq \sqrt{\frac{1}{2\bar{\rho}}} && \text{(from Equation (3.1))} \\
&= \sqrt{\sin \theta} \\
&\geq \sin \theta && (0 < \sin \theta < 1; \text{ therefore } \sqrt{\sin \theta} > \sin \theta)
\end{aligned}$$

yielding that  $\phi > 2\theta$ .

However, since  $t$  is a skinny triangle, its smallest angle must be no larger than  $\theta$ :  $\phi \leq \theta$ , a contradiction.  $\square$

**THEOREM 4.6 (Point Spacing Theorem).** *With the use of the GCDR algorithm either*

$$R(p_i) \geq C_n \cdot R(\hat{p}_i), \quad n = 1, 2, 3, \quad (4.6)$$

or

$$R(p_i) \geq C_n \cdot \text{lfs}(p_i), \quad n = 4, 5, \quad (4.7)$$

where  $C_n$  are defined separately for each of the cases (n) from Table 4.1 as follows:  $C_1 = \bar{\rho}\delta_2$ ,  $C_2 = \frac{\delta_1\sqrt{3}}{2}$ ,  $C_3 = \bar{\rho}\delta_1\sqrt{2\delta_2 - \delta_2^2}$ ,  $C_4 = \frac{\mu}{2\cos\alpha_{\min}}$ ,  $C_5 = \frac{\mu}{2-\mu}$ , where  $\alpha_{\min}$  is the minimum input angle of the PSLG.

*Proof.*

*Case (1)* By the definition of the parent vertex, Definition 2.5 (Rule-2),  $\hat{p}_i$  is the most recently inserted endpoint of the shortest edge of the triangle. Consider

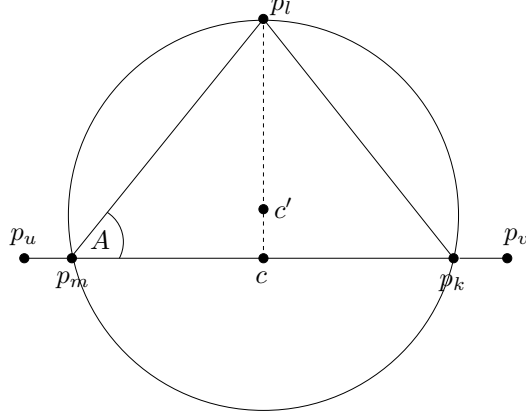


FIG. 4.3. Points  $c$  and  $c'$  are the centers of the encroached segment  $s = e(p_u p_v)$  and the circumcircle of the encroaching triangle  $t = \Delta p_m p_l p_k$  respectively. The endpoints of the separator of  $s$  (points  $p_k$  and  $p_m$ ) have moved exactly on  $s$ , while  $t$  is an isosceles triangle (with  $e(p_m p_k)$  being the base) maximizing in this way the upper bound of  $R(\hat{p}_i)$ .

Figure 3.1(left). Without loss of generality, let  $\hat{p}_i = p_l$  and  $e(p_l p_m)$  be the shortest edge of the skinny triangle  $\Delta p_k p_l p_m$  with circumradius  $r$ . Then

$$\begin{aligned}
 R(p_i) &\geq \delta_2 r && \text{(from Lemma 4.1)} \\
 &= \delta_2 \frac{r}{\|p_l - p_m\|} \|p_l - p_m\| \\
 &= \delta_2 \rho \|p_l - p_m\| \\
 &\geq \delta_2 \bar{\rho} \|p_l - p_m\| && \text{(since } \rho \geq \bar{\rho} \text{)} \\
 &\geq \delta_2 \bar{\rho} R(p_l) && \text{(from Remark 1)} \\
 &= \delta_2 \bar{\rho} R(\hat{p}_i);
 \end{aligned}$$

therefore, (4.6) holds with  $C_1 = \bar{\rho} \delta_2$ .

The argument above holds for all types of  $\hat{p}_i$ , because it does not involve the properties of  $\hat{p}_i$  specific for a particular type.

*Case (2)* See Figure 3.1(middle). In this case,  $p_i$  is a Type-B point inserted on an encroached, constrained segment  $s = e(p_u p_v)$ , and its parent  $\hat{p}_i$  is of Type-A. Therefore, Lemma 4.2 holds.

From the first part of Lemma 4.2, we have that there are no non-free vertices that are inside the diametral circle of  $s$  and visible from  $p_i$ . Therefore, by Definition 2.5 (Rule-3), the parent  $\hat{p}_i$  of  $p_i$  is the most recently inserted vertex of the shortest edge of the encroaching triangle  $t = \Delta p_k p_l p_m$ . By Lemma 4.5,  $e(p_m p_k)$  cannot be the shortest edge of  $t$ , since it is the separator of  $s$ . Therefore, the shortest edge of  $t$  is either  $e(p_l p_m)$  or  $e(p_l p_k)$ . If  $e(p_l p_m)$  is shorter than  $e(p_l p_k)$ , then the parent is the vertex  $p_l$  or  $p_m$ . In either case,  $R(\hat{p}_i) \leq \|p_l - p_m\|$  from Remark 1; otherwise,  $e(p_l p_k)$  is the shortest edge and thus the parent is the vertex  $p_l$  or  $p_k$ . In either case,  $R(\hat{p}_i) \leq \|p_l - p_k\|$  from Remark 1. Hence, no matter which exact vertex is the parent, we obtain that  $R(\hat{p}_i) \leq \min\{\|p_l - p_m\|, \|p_l - p_k\|\}$ .

Furthermore, from the second part of Lemma 4.2, we obtain that  $R(p_i) \geq \delta_1 \frac{\|p_u - p_v\|}{2}$  (inequality (4.2)).

We next try to find an upper bound for the ratio  $\frac{R(\hat{p}_i)}{R(p_i)}$ . Without loss of generality, assume that segment  $s$  has been rotated around its midpoint  $c$  in such a way that

the separator of  $s$  (i.e.,  $e(p_m p_k)$ ) is parallel to  $s$ , as depicted in Figure 3.1(middle). Note that this rotation does not change either the upper bound of  $R(\hat{p}_i)$  or the lower bound of  $R(p_i)$  because both the length of  $s$  and  $t$ 's vertices remain intact.

Keeping the lower bound of  $R(p_i)$  fixed (i.e., keeping the position of  $s$ 's endpoints fixed), we will first try to calculate what is the maximum value  $R(\hat{p}_i)$  can reach. See Figure 3.1(middle): by moving the endpoints of the edge  $e(p_m p_k)$  (the separator of the encroached segment) on  $t$ 's circumcircle and towards the encroached segment  $e(p_u p_v)$ ,  $R(\hat{p}_i)$  does not decrease, because the length of the edges  $e(p_l p_m)$  and  $e(p_l p_k)$  increases. Note that  $e(p_m p_k)$  can at most fall on  $e(p_u p_v)$ , since otherwise  $e(p_u p_v)$  would intersect the interior of  $t$ . Also, by moving appropriately the vertex  $p_l$  on the circle between the endpoints of  $e(p_m p_k)$ , we can turn  $t$  into an isosceles triangle, and therefore we can further increase the quantity  $\min\{\|p_l - p_m\|, \|p_l - p_k\|\}$ . See Figure 4.3 for an illustration.

$$\begin{aligned}
R(\hat{p}_i) &\leq \min\{\|p_l - p_m\|, \|p_l - p_k\|\} \\
&= \|p_l - p_m\| && \text{(since } t \text{ is turned into an isosceles triangle)} \\
&= \frac{\|p_m - c\|}{\cos A} && \text{(from the right triangle } \triangle p_m c p_l \text{ of Figure 4.3)} \\
&\leq \frac{\|p_u - p_v\|}{2 \cos A} \\
&\leq \frac{R(p)}{\delta_1 \cos A} && \text{(from inequality (4.2)).}
\end{aligned}$$

However, Lemma 4.5 also implies that the minimum angle of  $t$  is  $A$  and since  $t$  is a skinny triangle, we have that  $A \leq \theta$ . Therefore, we finally get that

$$R(\hat{p}_i) \leq \frac{R(p)}{\delta_1 \cos \theta}. \quad (4.8)$$

Since  $\theta$  is an acute angle, we obtain that:

$$\begin{aligned}
\cos \theta &= \sqrt{1 - \sin^2 \theta} \\
&= \sqrt{1 - \frac{1}{4\bar{\rho}^2}} && \text{(since } \sin \theta = \frac{1}{2\bar{\rho}} \text{ by definition)} \\
&\geq \sqrt{1 - \frac{1}{4}} && \text{(since } \bar{\rho} \geq 1 \text{ from Definition 3.1)} \\
&= \frac{\sqrt{3}}{2},
\end{aligned}$$

and inequality (4.8) becomes

$$R(\hat{p}_i) \leq \frac{2R(p)}{\delta_1 \sqrt{3}}.$$

Therefore, (4.6) holds with  $C_2 = \frac{\delta_1 \sqrt{3}}{2}$ .

*Case (3)* Let  $t$  be the triangle encroaching upon  $s$ ,  $l$  be its shortest edge, and  $r$  be its circumradius. From Remark 3, we have that  $\hat{p}_i$  is the most recently inserted vertex of  $l$ . Since  $t$  is a poor triangle,  $|l|$  can at most be equal to  $\frac{r}{\bar{\rho}}$ . Therefore, from Remark 1, we obtain that :

$$R(\hat{p}_i) \leq \frac{r}{\bar{\rho}}. \quad (4.9)$$

Also, notice that:

$$\begin{aligned}
R(p_i) &\geq \delta_1 \frac{|s|}{2} && \text{(from inequality (4.2))} \\
&\geq \delta_1 r \sqrt{2\delta_2 - \delta_2^2} && \text{(from inequality (4.5))} \\
&\geq \delta_1 \bar{\rho} R(\hat{p}_i) \sqrt{2\delta_2 - \delta_2^2} && \text{(from inequality (4.9)).}
\end{aligned}$$



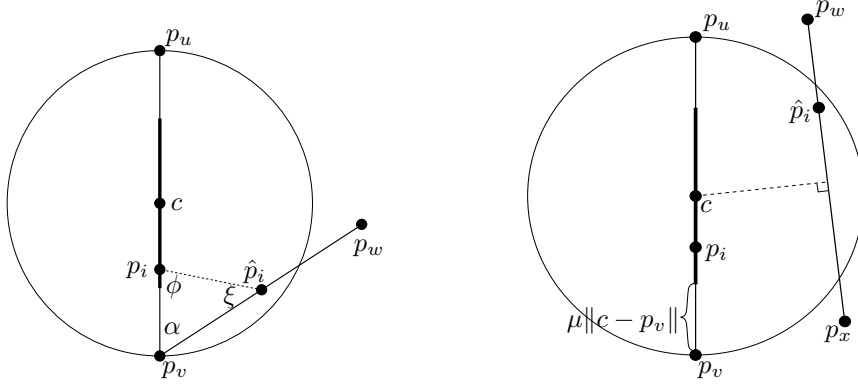


FIG. 4.4. Point  $p_i$  is a Type-C point inserted on the encroached segment  $s$ . Point  $\hat{p}_i$  is a non-external parent. Point  $c$  is not part of the mesh; it is an auxiliary point that denotes the center of the segments. (Left) Points  $p_i$  and  $\hat{p}_i$  lie on incident constrained segments separated by angle  $\alpha$ ,  $60^\circ \leq \alpha < 90^\circ$ . (case (4) from Table 4.1). (Right)  $p_i$  and  $\hat{p}_i$  lie on non-incident constrained segments (case (5) from Table 4.1).

Therefore, in this case, equation (4.6) holds with  $C_3 = \bar{\rho}\delta_1\sqrt{2\delta_2 - \delta_2^2}$ .

The argument above holds for each type of  $\hat{p}_i$  shown in Table 4.1, because it does not involve the properties of  $\hat{p}_i$  specific for a particular type.

Case (4) Since  $p_i$  is a Type-C point, Lemma 4.3 holds. Consider Figure 4.4(left). Based on Lemma 4.3, we separate 2 possibilities:

- (a) If the parent  $\hat{p}_i$  is the closest point to  $p_i$ , then

$$\begin{aligned} \frac{R(p_i)}{R(\hat{p}_i)} &= \frac{\|p_i - \hat{p}_i\|}{R(\hat{p}_i)} && \text{(from equation (4.3))} \\ &\geq \frac{\|p_i - \hat{p}_i\|}{\|p_i - p_v\|} && \text{(from Remark 1)} \\ &= \frac{\sin \alpha}{\sin \phi} && \text{(considering } \triangle p_i p_v \hat{p}_i \text{).} \end{aligned}$$

We wish to determine what values angle  $\phi$  can take. Since  $\|p_i - \hat{p}_i\| \leq \|p_i - p_v\|$  by our assumption, we get that  $\alpha \leq \xi$  from  $\triangle p_i p_v \hat{p}_i$ . Therefore,  $\phi \leq 180^\circ - 2\alpha$ . This implies that

$$\begin{aligned} \frac{R(p_i)}{R(\hat{p}_i)} &\geq \frac{\sin \alpha}{\sin (180 - 2\alpha)} \\ &= \frac{\sin \alpha}{\sin (2\alpha)} \\ &= \frac{\sin \alpha}{2 \sin \alpha \cos \alpha} \\ &= \frac{1}{2 \cos \alpha}, \end{aligned}$$

yielding that

$$R(p_i) \geq \frac{1}{2 \cos \alpha_{\min}} R(\hat{p}_i). \quad (4.10)$$

- (b) If an endpoint of the constrained encroached segment  $e(p_u p_v)$  is the closest point to  $p_i$ , then

$$\begin{aligned} \frac{R(p_i)}{R(\hat{p}_i)} &\geq \frac{\mu \frac{\|p_u - p_v\|}{2}}{R(\hat{p}_i)} && \text{(from inequality (4.4))} \\ &\geq \frac{\mu \|p_u - p_v\|}{2 \|p_i - p_v\|} && \text{(from Remark 1).} \end{aligned}$$

An upper bound for the distance  $\|\hat{p}_i - p_v\|$  is obtained when  $\hat{p}_i$  lies on the diametral circle of the segment  $e(p_u p_v)$  (in fact,  $\hat{p}_i$  cannot lie exactly on the

diametral circle, since it is a non-external vertex). From the isosceles triangle  $\triangle \hat{p}_i c p_v$  (see Figure 4.4(left)), we get that  $\|\hat{p}_i - p_v\| < \|p_u - p_v\| \cos \alpha$ , and therefore

$$\begin{aligned} \frac{R(p_i)}{R(\hat{p}_i)} &> \frac{\mu \|p_u - p_v\|}{2 \|p_u - p_v\| \cos \alpha} \\ &= \frac{\mu}{2 \cos \alpha}, \end{aligned}$$

obtaining in this case that

$$R(p_i) > \frac{\mu}{2 \cos \alpha_{\min}} R(\hat{p}_i). \quad (4.11)$$

In both cases,  $C_4 = \frac{\mu}{2 \cos \alpha_{\min}}$  satisfies both equation (4.10) and (4.11), and thus (4.6) holds.

The argument above holds for each type of  $\hat{p}_i$  shown in Table 4.1, because it does not involve the properties of  $\hat{p}_i$  specific for a particular type.

*Case (5)* See Figure 4.4(right). Based on Lemma 4.3, we, again, separate two possibilities:

- (a) If  $\hat{p}_i$  is the vertex closest to  $p_i$ , then, from equation (4.3),  $R(p_i) = \|p_i - \hat{p}_i\|$ . Since, however,  $p_i$  and  $\hat{p}_i$  lie on non-incident features, we obtain that  $\text{lfs}(p_i) \leq \|p_i - \hat{p}_i\|$  (see Definition 2.2), yielding that  $R(p_i) \geq \text{lfs}(p_i)$ .
- (b) Otherwise, an endpoint of the constrained encroached segment  $e(p_u p_v)$  is the closest point to  $p_i$ . Then, if  $c$  is the center of  $s$ , by Definition 2.2 of the lfs () function,

$$\text{lfs}(c) \leq \|c - \hat{p}_i\|. \quad (4.12)$$

Therefore,

$$\begin{aligned} \text{lfs}(p_i) &\leq \text{lfs}(c) + \|p_i - c\| && \text{(from Lemma 2.3)} \\ &\leq \|c - \hat{p}_i\| + \|p_i - c\| && \text{(from (4.12))} \\ &\leq \frac{|s|}{2} + \|p_i - c\| && \text{(because } \hat{p}_i \text{ is inside the diametral circle of } s) \\ &\leq \frac{|s|}{2} + (1 - \mu) \frac{|s|}{2} && \text{(since } p_i \text{ lies in the Type-C selection interval of } s) \\ &= (2 - \mu) \frac{|s|}{2} \\ &\leq (2 - \mu) \frac{R(p_i)}{\mu} && \text{(from inequality (4.4)).} \end{aligned}$$

In both cases,  $C_5 = \frac{\mu}{2 - \mu}$  satisfies the inequality (4.7).

The argument above holds for each type of  $\hat{p}_i$  shown in Table 4.1, because it does not involve the properties of  $\hat{p}_i$  specific for a particular type.  $\square$

**5. Proof of Good Grading.** The main result of this section is Theorem 5.5 which proves that GCDR produces well-graded triangles. Theorem 5.5 will also allow us to prove termination, since it is possible to bound from below the closest distance of any two visible vertices. Notice that we first prove good grading and then we prove termination.

First, we prove Lemmas 5.1, 5.2, and 5.3 that bound from above the distance from a point to its parent in terms of the size of the corresponding two-dimensional and one-dimensional selection region, respectively. These results are used to prove Lemma 5.4 which shows that the vertex density in a point is bounded from above by a linear function of the density in its parent. Lemma 5.4 is proved only for cases (1)–(4), since for case (5) the relation of the insertion radius to the local feature size



Conversely, keeping the position of  $c$  fixed, we are trying to decrease  $|s|$  by moving only the endpoints of  $s$ : the length of  $s$  reaches its smallest value when  $s$  is tangent to the selection circle, and one of its endpoints—say the point  $p_u$ —lies precisely on the circumcircle. See Figure 5.1 for an illustration. Note that if  $s$  did not intersect the selection circle at all, then the first part of Lemma 4.4 would be violated: a contradiction.

From the right triangle  $\triangle cdc'$  (see Figure 5.1), we obtain that:

$$\begin{aligned} \|c - c'\|^2 &= \|d - c'\|^2 + \|c - d\|^2 \\ &= r^2(1 - \delta_2)^2 + \|c - d\|^2 \\ &= r^2(1 - \delta_2)^2 + \left(\frac{|s|}{2} - \|p_u - d\|\right)^2 \\ &= r^2(1 - \delta_2)^2 + \left(\frac{|s|}{2} - r\sqrt{2\delta_2 - \delta_2^2}\right)^2 \quad (\text{from the right triangle } \triangle kdp_u) \\ &= r^2 + \frac{|s|^2}{4} - r|s|\sqrt{2\delta_2 - \delta_2^2}, \end{aligned}$$

yielding that:

$$\|c - c'\| = \sqrt{r^2 + \frac{|s|^2}{4} - r|s|\sqrt{2\delta_2 - \delta_2^2}}. \quad (5.3)$$

We also have that:

$$\begin{aligned} \frac{\|c - \hat{p}\|}{|s|} &= \frac{r + \|c - c'\|}{|s|} \quad (\text{since } c, \hat{p} \text{ and } c' \text{ are collinear}) \\ &= \frac{r + \sqrt{r^2 + \frac{|s|^2}{4} - r|s|\sqrt{2\delta_2 - \delta_2^2}}}{|s|} \quad (\text{from Equation (5.3)}), \end{aligned}$$

and after the simplification, we finally get that:

$$\frac{\|c - \hat{p}\|}{|s|} = \left(\frac{r}{|s|}\right) + \sqrt{\left(\frac{r}{|s|}\right)^2 + \frac{1}{4} - \left(\frac{r}{|s|}\right)\sqrt{2\delta_2 - \delta_2^2}}. \quad (5.4)$$

Basic calculus, however, reveals that the right-hand part of Equation (5.4) is an always increasing function with respect to the “variable”  $\frac{r}{|s|}$ . Also, from inequality (4.5), we already know that  $\frac{r}{|s|} \leq \frac{1}{2\sqrt{2\delta_2 - \delta_2^2}}$ . Thus, by replacing  $\frac{r}{|s|}$  in the right-hand part of Equation (5.4) with its largest value and simplifying the result, we get that:

$$\frac{\|c - \hat{p}\|}{|s|} \leq \frac{1}{2} \sqrt{\frac{2 - \delta_2}{\delta_2}}. \quad (5.5)$$

Lastly, the desired outcome follows:

$$\begin{aligned} \|p - \hat{p}\| &\leq \|p - c\| + \|c - \hat{p}\| \quad (\text{from the triangle inequality}) \\ &\leq (1 - \delta_1) \frac{|s|}{2} + \|c - \hat{p}\| \quad (\text{since } p \text{ is in the Type-B selection interval}) \\ &\leq (1 - \delta_1) \frac{|s|}{2} + \frac{|s|}{2} \sqrt{\frac{2 - \delta_2}{\delta_2}} \quad (\text{from Equation (5.5)}) \\ &= \left(1 + \sqrt{\frac{2 - \delta_2}{\delta_2}} - \delta_1\right) \frac{|s|}{2}. \end{aligned}$$

□

LEMMA 5.3. *If  $p_i$  is of Type-C, then*

$$\|p_i - \hat{p}_i\| \leq (2 - \mu) \frac{|s|}{2}, \quad (5.6)$$

where  $|s|$  is the length of the encroached segment  $s$ .

*Proof.* If  $c$  is the center of  $s$ , then

$$\begin{aligned} \|p_i - \hat{p}_i\| &\leq \|p_i - c\| + \|c - \hat{p}_i\| && \text{(from the triangle inequality)} \\ &\leq (1 - \mu) \frac{|s|}{2} + \|c - \hat{p}_i\| && \text{(since } p_i \text{ is in the Type-C selection interval)} \\ &\leq (1 - \mu) \frac{|s|}{2} + \frac{|s|}{2} && \text{(since } \hat{p}_i \text{ is a non-external parent)} \\ &= (2 - \mu) \frac{|s|}{2}. \end{aligned}$$

□

LEMMA 5.4. *If  $p$  is a vertex of the mesh inserted by the GCDR algorithm, and  $C_n$  ( $n = 1, 2, 3, 4$ ) are the constants specified by Theorem 4.6 for the corresponding cases listed in Table 4.1, then the following inequality holds:*

$$D(p) \leq B_n + \frac{D(\hat{p})}{C_n}, \quad n = 1, 2, 3, 4 \quad (5.7)$$

where  $B_1 = \frac{2-\delta_2}{\delta_2}$ ,  $B_2 = B_3 = \frac{1+\sqrt{\frac{2-\delta_2}{\delta_2}-\delta_1}}{\delta_1}$ ,  $B_4 = \frac{2-\mu}{\mu}$ .

*Proof.*

First, we prove the inequality

$$\|p - \hat{p}\| \leq B_n \cdot R(p) \quad (5.8)$$

for each of the cases below.

*Case (1):*

$$\begin{aligned} \|p - \hat{p}\| &\leq (2 - \delta_2)r && \text{(from Lemma 5.1)} \\ &= \frac{2-\delta_2}{\delta_2} \delta_2 r \\ &\leq \frac{2-\delta_2}{\delta_2} R(p) && \text{(from Lemma 4.1);} \end{aligned}$$

therefore, inequality (5.8) can be satisfied with  $B_1 = \frac{2-\delta_2}{\delta_2}$ .

*Case (2):* In this case,  $p_i$  is of Type-B and its parent  $\hat{p}_i$  is a Type-A point. We assume that  $p_i$  is an external parent, since if it was a non-external parent, the distance between  $p_i$  and  $\hat{p}_i$  would be smaller.

$$\begin{aligned} \|p - \hat{p}\| &\leq \left(1 + \sqrt{\frac{2-\delta_2}{\delta_2} - \delta_1}\right) \frac{|s|}{2} && \text{(from Lemma 5.2)} \\ &= \frac{1 + \sqrt{\frac{2-\delta_2}{\delta_2} - \delta_1}}{\delta_1} \delta_1 \frac{|s|}{2} \\ &\leq \frac{1 + \sqrt{\frac{2-\delta_2}{\delta_2} - \delta_1}}{\delta_1} R(p) && \text{(from inequality (4.2));} \end{aligned}$$

therefore, inequality (5.8) can be satisfied with  $B_2 = \frac{1 + \sqrt{\frac{2-\delta_2}{\delta_2} - \delta_1}}{\delta_1}$ .

*Case (3):* The analysis is exactly the same as in case (2), since  $p_i$  is a Type-B point, and  $\hat{p}_i$  is an external parent. Therefore, inequality (5.8) can be satisfied with  $B_3 = B_2$ .

*Case (4):* Based on Lemma 4.3, we separate two possibilities:

- (a) If  $\hat{p}_i$  is closest to  $p_i$ , then  $\|p_i - \hat{p}_i\| = R(p_i)$  from equality (4.3).
- (b) If an endpoint of  $s$  is closest to  $p_i$ , then

$$\begin{aligned} \|p_i - \hat{p}_i\| &\leq (2 - \mu) \frac{|s|}{2} && \text{(from Lemma 5.3)} \\ &= \frac{2-\mu}{\mu} \mu \frac{|s|}{2} \\ &\leq \frac{2-\mu}{\mu} R(p_i) && \text{(from inequality (4.3));} \end{aligned}$$

therefore, inequality (5.8) can be satisfied with  $B_4 = \frac{2-\mu}{\mu}$  in both cases.

Now, for all cases (1)–(4),

$$\begin{aligned} \text{lfs}(p) &\leq \text{lfs}(\hat{p}) + \|p - \hat{p}\| && \text{(from Lemma 2.3)} \\ &\leq \text{lfs}(\hat{p}) + B_n R(p) && \text{(from (5.8))} \\ &= D(\hat{p}) R(\hat{p}) + B_n R(p) && \text{(from (2.2))} \\ &\leq D(\hat{p}) \frac{R(p)}{C_n} + B_n R(p) && \text{(from Theorem 4.6).} \end{aligned}$$

The result follows from the division of both sides by  $R(p)$ .  $\square$

**THEOREM 5.5.** *Suppose that the following five inequalities hold:*

**I-1.**  $\bar{\rho} > 1$  (implying a lower angle bound arbitrarily close to  $30^\circ$ ),

**I-2.**  $\alpha_{\min} > 60^\circ$  (recall that  $\alpha_{\min}$  is the smallest input angle),

**I-3.**  $\delta_2 > \frac{1}{\bar{\rho}}$ ,

**I-4.**  $\delta_1 > \frac{1}{\bar{\rho}}$ , and

**I-5.**  $\mu > 2 \cos \alpha_{\min}$ .

Then, there exist fixed constants  $D_A \geq 1$ ,  $D_B \geq 1$ , and  $D_C \geq 1$  such that, for any vertex  $p$  inserted by the GCDR algorithm, the following inequalities hold:

$$D(p) \leq \begin{cases} D_A & \text{if } p \text{ is of Type-A,} \\ D_B & \text{if } p \text{ is of Type-B,} \\ D_C & \text{if } p \text{ is of Type-C.} \end{cases} \quad (5.9)$$

Therefore, the insertion radius of  $p$  has a lower bound proportional to its local feature size.

*Proof.* First of all, observe that there are legal values for the parameters  $\delta_2, \delta_1$ , and  $\mu$  that satisfy inequalities I-1, I-2, I-3, I-4, and I-5. In fact, the parameters satisfy these inequalities if they are assigned to any value other than their minimum possible value as defined in Definition 3.1 (selection circles), Definition 3.2 (Type-B selection intervals), and Definition 3.3 (Type-B selection intervals), respectively.

The proof is by induction and is similar to the proof of Lemma 7 in [21]. The base case covers the input vertices, and the inductive step covers the other three types of vertices.

*Base case:* The theorem is true if  $p$  is an input vertex, because in this case, by Remark 2,  $D(p) = \text{lfs}(p) / R(p) \leq 1$ .

*Inductive hypothesis:* Assume that the theorem is true for  $\hat{p}$ , i.e.,

$$D(\hat{p}) \leq \begin{cases} D_A & \text{if } \hat{p} \text{ is of Type-A,} \\ D_B & \text{if } \hat{p} \text{ is of Type-B,} \\ D_C & \text{if } \hat{p} \text{ is of Type-C.} \end{cases} \quad (5.10)$$

*Inductive step:* For each of the cases ( $n$ ),  $n = 1, 2, 3, 4$ , we start with (5.7) and apply the inductive hypothesis considering the possible type combinations of  $p$  and  $\hat{p}$  from Table 4.1. As a result, the inequalities in (5.9) can be satisfied if  $D_A$ ,  $D_B$ , and  $D_C$  are chosen such that the following inequalities (5.11), (5.12), (5.13), (5.14), (5.15), (5.16), (5.17), and (5.18) hold:

*Case (1):*

$$B_1 + \frac{D_A}{C_1} \leq D_A, \quad (5.11)$$

$$B_1 + \frac{D_B}{C_1} \leq D_A, \quad (5.12)$$

$$B_1 + \frac{D_C}{C_1} \leq D_A, \quad (5.13)$$

Case (2):

$$B_2 + \frac{D_A}{C_2} \leq D_B, \quad (5.14)$$

Case (3):

$$B_3 + \frac{D_B}{C_3} \leq D_B, \quad (5.15)$$

$$B_3 + \frac{D_C}{C_3} \leq D_B, \quad (5.16)$$

Case (4):

$$B_4 + \frac{D_B}{C_4} \leq D_C, \quad (5.17)$$

$$B_4 + \frac{D_C}{C_4} \leq D_C, \quad (5.18)$$

For case (5), from Theorem 4.6, we have:  $D(p) = \text{lfs}(p)/R(p) \leq 1/C_5$ , i.e., the inequalities in (5.9) can be satisfied if  $D_C$  is chosen such that the following inequality holds:

Case (5):

$$\frac{1}{C_5} = B_4 \leq D_C, \quad (5.19)$$

Notice that since  $B_n \geq 1$  for every  $n = 1, 2, 3, 4$ , the solution of the system above guarantees that  $D_A, D_B, D_C$  are larger than or equal to 1.

From (5.11), we obtain that:

$$D_A \geq \frac{B_1 C_1}{C_1 - 1}. \quad (5.20)$$

From (5.15), we obtain that:

$$D_B \geq \frac{B_3 C_3}{C_3 - 1}. \quad (5.21)$$

Also, from (5.18), we have that:

$$D_C \geq \frac{B_4 C_4}{C_4 - 1}. \quad (5.22)$$

Finally, from (5.12), (5.13), (5.14), (5.16), (5.17), (5.19), (5.20), (5.21), and (5.22), we obtain the solution:

$$\begin{aligned} D_A &\geq \max \left\{ \frac{B_1 C_1}{C_1 - 1}, \frac{B_3 C_3}{C_3 - 1} + B_1, \frac{B_4 C_4}{C_4 - 1} + B_1 \right\}, \\ D_B &\geq \max \left\{ \frac{B_3 C_3}{C_3 - 1}, \frac{B_1 C_1}{C_2(C_1 - 1)} + B_2, \frac{B_4 C_4}{C_3(C_4 - 1)} + B_3 \right\}, \\ D_C &\geq \max \left\{ \frac{B_4 C_4}{C_4 - 1}, \frac{B_3 C_3}{C_4(C_3 - 1)} + B_4, B_4 \right\}. \end{aligned} \quad (5.23)$$

If we plug in the values for  $B_n$  and  $C_n$ , we have:

$$\begin{aligned} D_A &\geq \frac{2-\delta_2}{\delta_2} + \max \left\{ \frac{2-\delta_2}{\delta_2(\bar{\rho}\delta_2-1)}, \frac{(2-\delta_2+(1-\delta_1)\sqrt{2\delta_2-\delta_2^2})}{\delta_2(\bar{\rho}\delta_1\sqrt{2\delta_2-\delta_2^2}-1)}, \frac{2-\mu}{\bar{\rho}\delta_2(\mu-2\cos\alpha_{\min})} \right\}, \\ D_B &\geq \frac{1+\sqrt{\frac{2-\delta_2}{\delta_2}-\delta_1}}{\delta_1} + \max \left\{ \frac{1+\sqrt{\frac{2-\delta_2}{\delta_2}-\delta_1}}{\delta_1(\bar{\rho}\delta_1\sqrt{2\delta_2-\delta_2^2}-1)}, \frac{\bar{\rho}(2-\delta_2)2}{\delta_1(\bar{\rho}\delta_2-1)\sqrt{3}}, \frac{2-\mu}{\bar{\rho}\delta_1\sqrt{2\delta_2-\delta_2^2}(\mu-2\cos\alpha_{\min})} \right\}, \\ D_C &\geq \frac{2-\mu}{\mu} + \max \left\{ \frac{2(2-\mu)\cos\alpha_{\min}}{\mu(\mu-2\cos\alpha_{\min})}, \frac{2\bar{\rho}\cos\alpha_{\min}(1+\sqrt{\frac{2-\delta_2}{\delta_2}-\delta_1})\sqrt{2\delta_2-\delta_2^2}}{\mu(\bar{\rho}\delta_1\sqrt{2\delta_2-\delta_2^2}-1)} \right\}. \end{aligned}$$

Note that the inequalities I-1, I-2, I-3, I-4, and I-5 guarantee that the grading constants  $D_A, D_B$ , and  $D_C$  are well defined, i.e., they are not infinite.  $\square$

The area (size) of the selection regions affects the grading of our algorithm, theoretically at least. Indeed, if either of the parameters  $\delta_1, \delta_2, \mu$  decreases (thus increasing the area of the selection regions), then the lower bounds for the constants  $D_A, D_B, D_C$  of Theorem 5.5 increase making the grading worse. In practice, when we increase the area of the selection regions, the deterioration of grading is less severe (see Section 7).

**6. Proof of Termination.** The good grading of GCDR implies termination as well. For reasons of completeness, however, we present a concrete proof.

**THEOREM 6.1.** *GCDR terminates producing triangles with angles arbitrarily close to  $30^\circ$ .*

*Proof.* To prove termination, it suffices to prove that no two vertices, visible to each other, are closer than a real constant  $C' > 0$ , since the insertion of an infinite number of vertices would necessarily introduce at some point two visible vertices closer than  $C'$ . From Remark 1, however, the distance of any two visible vertices is bounded from below by the insertion radius of one of these vertices. Therefore, it is adequate to prove that the insertion radius of any point is not less than the positive, real constant  $C'$ .

Table 4.1 presents an exhaustive enumeration of all possible parent-child combinations. First, we prove by contradiction that the combinations marked as “n/a” cannot arise. These combinations can occur in the following two cases:

1. A Type-B point  $p_i$  lies on an encroached segment  $s$ , and its parent is a non-free non-external vertex, i.e.,  $\hat{p}_i$  is a non-free point that lies strictly inside the diametral circle of  $s$ . Recall that the parent of any point  $p_i$  is visible from  $p_i$  (see Lemma 2.6). By the way we defined Type-B points, however, there is no non-free vertex strictly inside the diametral circle of  $s$  and visible from  $p_i$ : a contradiction.



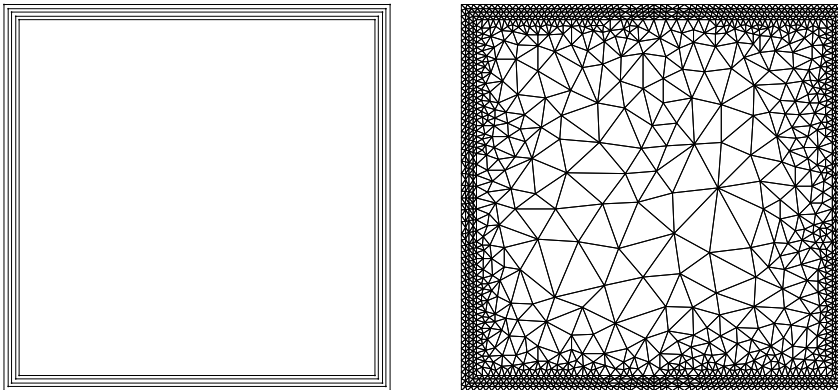


FIG. 7.1. *(Left)* The input PSLG used for the experiments. It consists of 5 concentric squares. The horizontal and vertical distance between two adjacent squares is one hundredth of the side length of the outer-most square. *(Right)* The output mesh obtained by GCDR on the input PSLG with  $\bar{\rho}$  being set to 1. GCDR terminates producing 3200 triangles whose angles are more than  $30^\circ$ .

2. A Type-C point  $p_i$  lies on an encroached segment  $s$ , and its parent is either a free vertex or a non-free external parent. By the way we defined Type-C points, the diametral circle of  $s$  contains at least one non-free vertex visible from  $p_i$ . Therefore, from Definition 2.5 (Rule-4), the parent of  $p_i$  is the closest-to- $p_i$ , non-free vertex that lies inside the diametral circle of  $s$  and is visible from  $p_i$ . This means that  $p_i$  can be neither a free vertex nor an external parent: a contradiction.

All the remaining parent-child combinations (marked with numbers) have been analyzed in Theorem 5.5. From that theorem it follows that with the use of the GCDR algorithm the insertion radius of any vertex is no less than  $C' = \frac{\text{lfs}_{\min}}{\max\{D_A, D_B, D_C\}}$ , where  $\text{lfs}_{\min} = \min_{p \in \Omega} \text{lfs}(p) > 0$ . Note that inequalities I-1, I-2, I-3, I-4, and I-5 of Theorem 5.5 imply that the positive constants  $D_A, D_B, D_C$  cannot approach infinity, and therefore  $C'$  is a positive real number.  $\square$

**7. Experimental Evaluation.** In this section, we experimentally evaluate the grading achieved by GCDR. We have implemented GCDR on top of the Computational Geometry Algorithms Library (CGAL) [1]. For the visualization of the mesh, we used the C++ Visualization Toolkit Library (VTK) [2].

The input PSLG used for the experiments is depicted in Figure 7.1. Other input PSLGs yielded similar results.

We conducted two experiments denoted as Experiment-1 and Experiment-2 respectively. In the Experiment-1, we executed GCDR 32 times. At every execution, we changed the size of the selection regions by altering the values of the parameters  $\delta_2, \delta_1$ , and  $\mu$ . Also, for each execution, all the Steiner points inserted (or considered for insertion) by GCDR lied exactly on the boundary of selection circles or selection intervals. More precisely, every Type-A Steiner point is inserted as close to an arbitrary vertex of the corresponding skinny triangle as possible, and every Type-B/Type-C Steiner point is inserted as close to an arbitrary endpoint of the corresponding encroached segment as possible. In this way, we test our algorithm when the inserted Steiner points lie in extreme positions.

Table 7.1 summarizes the results for the first experiment under the label “Experi-

Configuration Id							Experiment-1				Experiment-2		
	$\delta_2$	$\delta_1$	$\mu$	$D_A$	$D_B$	$D_C$	$\max_{p \text{ is Type-A}} D(p)$	$\max_{p \text{ is Type-B}} D(p)$	$\max_{p \text{ is Type-C}} D(p)$	Number of triangles	$\max_{p \text{ is Type-A}} D(p)$	$\max_{p \text{ is Type-B}} D(p)$	$\max_{p \text{ is Type-C}} D(p)$
1	1.00	1.00	1.00	3.41	4.94	1.00	1.93	0.70	1.00	1583	1.93	0.70	1.00
2	1.00	1.00	0.80	3.41	4.94	1.50	1.75	0.68	1.00	1814	2.21	0.74	1.00
3	1.00	1.00	0.60	3.41	4.94	2.33	2.19	0.70	1.15	2052	2.41	0.74	1.20
4	1.00	1.00	0.40	3.83	4.94	4.00	2.20	1.01	1.99	2557	2.49	1.09	2.19
5	1.00	0.90	1.00	5.03	5.70	1.00	1.60	0.79	1.00	1571	1.99	0.80	1.00
6	1.00	0.90	0.80	5.03	5.70	1.50	1.48	0.76	1.00	1804	2.19	0.79	1.00
7	1.00	0.90	0.60	5.03	5.70	2.33	2.02	0.78	1.15	2047	2.35	0.80	1.19
8	1.00	0.90	0.40	5.03	5.70	4.00	2.23	0.86	1.66	2546	2.50	1.15	2.06
9	1.00	0.80	1.00	10.13	12.92	1.00	1.60	0.87	1.00	1565	1.85	0.89	1.00
10	1.00	0.80	0.80	10.13	12.92	1.50	1.95	0.86	1.00	1818	2.18	0.91	1.00
11	1.00	0.80	0.60	10.13	12.92	2.33	2.02	0.88	1.15	2047	2.64	0.90	1.22
12	1.00	0.80	0.40	10.13	12.92	4.00	2.37	0.97	1.69	2505	2.48	1.61	2.11
13	0.90	1.00	1.00	5.70	7.69	1.00	2.26	0.70	1.00	1586	2.41	0.70	1.00
14	0.90	1.00	0.80	5.70	7.69	1.50	1.99	0.71	1.00	1799	2.57	0.76	1.00
15	0.90	1.00	0.60	5.70	7.69	2.33	2.63	0.70	1.15	2055	2.63	0.76	1.24
16	0.90	1.00	0.40	5.70	7.69	4.00	2.61	1.01	1.95	2595	2.62	1.02	2.26
17	0.90	0.90	1.00	6.22	8.66	1.00	2.04	0.77	1.00	1540	2.70	0.82	1.00
18	0.90	0.90	0.80	6.22	8.66	1.50	1.98	0.76	1.00	1807	2.49	0.81	1.00
19	0.90	0.90	0.60	6.22	8.66	2.33	2.79	0.78	1.15	2083	2.79	0.83	1.20
20	0.90	0.90	0.40	6.22	8.66	4.00	2.60	1.07	1.93	2578	2.84	1.40	2.13
21	0.90	0.80	1.00	12.70	14.61	1.00	2.47	0.87	1.00	1541	2.47	0.92	1.00
22	0.90	0.80	0.80	12.70	14.61	1.50	2.53	0.87	1.00	1811	2.56	0.92	1.00
23	0.90	0.80	0.60	12.70	14.61	2.33	2.79	0.88	1.15	2091	2.57	0.91	1.20
24	0.90	0.80	0.40	12.70	14.61	4.00	2.52	1.21	1.93	2540	2.71	1.25	1.94
25	0.80	1.00	1.00	12.92	16.14	1.00	2.71	0.70	1.00	1615	2.81	0.70	1.00
26	0.80	1.00	0.80	12.92	16.14	1.50	4.32	0.71	1.00	1868	4.32	0.78	1.00
27	0.80	1.00	0.60	12.92	16.14	2.33	3.65	0.70	1.15	2139	3.65	0.78	1.20
28	0.80	1.00	0.40	12.92	16.14	4.00	3.73	0.97	1.95	2628	3.54	1.35	2.10
29	0.80	0.90	1.00	12.92	18.05	1.00	2.46	0.77	1.00	1562	3.15	0.84	1.00
30	0.80	0.90	0.80	12.92	18.05	1.50	3.47	0.76	1.00	1843	2.96	0.85	1.00
31	0.80	0.90	0.60	12.92	18.05	2.33	3.53	0.83	1.15	2118	2.90	0.83	1.21
32	0.80	0.90	0.40	12.92	18.05	4.00	3.31	1.07	1.93	2615	3.26	1.23	1.95

TABLE 7.1

The 32 configurations used by Experiment-1 and Experiment-2. The results are shown in the last 7 columns.

ment-1". The quality upper bound is set to  $\bar{\rho} = \sqrt{2}$  which means that  $\delta_2 \geq \frac{1}{\sqrt{2}} \approx 0.71$  and that  $\delta_1 \geq \frac{0.71}{\delta_2}$ . Since  $\alpha_{\min} = 90^\circ$ , we also have that  $\mu \geq 0$ . Each row of the table corresponds to a specific execution where the values for the parameters are shown in the second, third, and fourth cell of each row. The table reports the largest density observed in practice per point type: the largest density observed among Type-A points (8<sup>th</sup> column), among Type-B (9<sup>th</sup> column), and among Type-C points (10<sup>th</sup> column). For comparison, the table also depicts (at the 5<sup>th</sup>, 6<sup>th</sup>, and 7<sup>th</sup> column) the tightest

theoretical upper bound of the density per point type for the respective configuration, as calculated in inequality (5.23) of Theorem 5.5.

The observed largest densities of Experiment-1 should be less than their theoretical counterparts. Indeed, the grading achieved in practice is much smaller than the theoretical bound of Theorem 5.5. This fact verifies the theory and also implies that GCDR behaves much better than theory suggests.

Also, notice that the densities of Type-C points seem to strongly affect the size of the output mesh. Indeed, at every execution where the maximum density of Type-C points exceeds 1.00, the number of triangles is more than 2,000. On the contrary, high grading of Type-A points (e.g., 26<sup>th</sup> execution) or high grading of Type-B points (e.g., 9<sup>th</sup> execution) do not result in a high size output mesh. This fact is attributable to the high number of Type-C points: in all the executions, the number of Type-C points (inserted into the mesh) is 3 to 4 times more than the combined number of Type-A and Type-B points.

Lastly, observe that each parameter seems to deteriorate the density of points of a certain type. Specifically, the decrease of  $\delta_2$  leads to a higher density of Type-A points, the decrease of  $\delta_1$  leads to a higher density of Type-B points, and the decrease of  $\mu$  leads to a higher density of Type-C points. This should be expected, since the parameters  $\delta_2$ ,  $\delta_1$ , and  $\mu$  determine the size of the selection regions of Type-A, Type-B, and Type-C points respectively.

Although the Steiner points, in the Experiment-1, are inserted in extreme positions, it is not certain whether the measured maximum densities are the worst. For example, see the 2<sup>nd</sup> configuration under the label Experiment-1: Type-C Steiner points lie farther from the center of the encroached segments than they do in the 1<sup>st</sup> configuration, but the maximum practical densities observed do not increase.

Therefore, we conducted another experiment which could potentially generate the highest (i.e., worst) practical densities. The results are illustrated in Table 7.1 under the label “Experiment-2”. Here, each configuration of the previous experiment is repeated for 100 times (and not just once as before). Each time, the Steiner points inserted were randomly chosen from within their corresponding selection region (i.e., they do not always lie on the boundary of the selection regions as before). We report the highest density per point type among the densities observed during the 100 repetitions.

The maximum densities measured in Experiment-2 are slightly higher than before, but still less than the theoretical counterparts. These observations further verify the theory and suggest that GCDR behaves much better in practice.

**8. Conclusions and Future Work.** We have presented and implemented a constrained Delaunay refinement algorithm in two dimensions. Our algorithm is more flexible than the traditional approaches, since the user can choose which Steiner point to insert into the mesh among an infinite, enumerable number of choices. Our algorithm significantly increases the number of these choices over our previous Generalized algorithms [4–7]. The flexibility offered by Generalized algorithms can benefit sliver removal in three dimensions [10, 15], since the area from which Steiner points are selected now increases potentially allowing to achieve even better dihedral angles. These customizable point insertion strategies offered by our algorithm can also help in boundary recovery by inserting, for instance, points on the boundary while refining the mesh. Other applications of Generalized algorithms can be found in [7].

Furthermore, this paper improves the quality guarantees: we have proved that our algorithm terminates and preserves good grading for a lower angle bound  $\theta$  arbitrarily

close to  $30^\circ$ . Experimental evaluation of our algorithm verified the theory.

The parallelization of our Generalized algorithm is left as future work. A parallel Generalized algorithm would automatically imply the parallelization of any point insertion strategy as long as the Steiner points lie in the selection regions.

Lastly, we wish to implement our algorithm in three dimensions and identify point insertion strategies suitable for sliver removal.

**9. Acknowledgments.** We thank the anonymous reviewers from the SISC journal whose insightful comments on our paper [7] motivated some of the research presented in this manuscript. This work was supported (in part) by the NSF grants CCF-0916526, CCS-0750901, and CCF-0833081, and by the John Simon Guggenheim Foundation.

#### References.

- [1] CGAL, *Computational Geometry Algorithms Library*. <http://www.cgal.org>.
- [2] VTK, *Visualization Toolkit*. <http://www.vtk.org>.
- [3] ADRIAN BOWYER, *Computing Dirichlet tessellations*, Computer Journal, 24 (1981), pp. 162–166.
- [4] ANDREY N. CHERNIKOV AND NIKOS P. CHRISOCHOIDES, *Generalized Delaunay Mesh Refinement: From Scalar to Parallel*, in Proceedings of the 15<sup>th</sup> International Meshing Roundtable, Birmingham, AL, September 2006, Elsevier.
- [5] ———, *Three-dimensional semi-generalized point placement method for Delaunay mesh refinement*, in Proceedings of the 16th International Meshing Roundtable, Seattle, WA, Oct. 2007, Springer, pp. 25–44.
- [6] ———, *Three-Dimensional Delaunay Refinement for Multi-Core Processors*, in Proceedings of the 22<sup>nd</sup> ACM International Conference on Supercomputing, Island of Kos, Greece, June 2008.
- [7] ———, *Generalized Two-Dimensional Delaunay Mesh Refinement*, SIAM Journal on Scientific Computing, 31 (2009), pp. 3387–3403.
- [8] L. PAUL CHEW, *Guaranteed-quality triangular meshes*, Tech. Report TR89983, Cornell University, Computer Science Department, 1989.
- [9] ———, *Guaranteed quality mesh generation for curved surfaces*, in Proceedings of the 9th ACM Symposium on Computational Geometry, San Diego, CA, 1993, pp. 274–280.
- [10] ———, *Guaranteed-quality Delaunay meshing in 3D*, in Proceedings of the 13<sup>th</sup> ACM Symposium on Computational Geometry, Nice, France, 1997, pp. 391–393.
- [11] HALE ERTEN AND ALPER ÜNGÖR, *Triangulations with locally optimal steiner points*, in SGP '07: Proceedings of the fifth Eurographics symposium on Geometry processing, Aire-la-Ville, Switzerland, Switzerland, 2007, Eurographics Association, pp. 143–152.
- [12] LORI A. FREITAG AND CARL OLLIVIER-GOOCH, *A Cost/Benefit Analysis of Simplicial Mesh Improvement Techniques as Measured by Solution Efficiency*, Preprint ANL/MCS-P722-0598, Mathematics and Computer Science Division, Argonne National Laboratory, Argonne, Ill, 10 (2000).
- [13] PAUL-LOUIS GEORGE AND HOUMAN BOROUCHE, *Delaunay Triangulation and Meshing. Application to Finite Elements*, HERMES, 1998.
- [14] BENOÎT HUDSON, *Safe Steiner Points for Delaunay Refinement*, in International Meshing Roundtable Research Notes, 2008.
- [15] XIANG-YANG LI, *Generating well-shaped d-dimensional Delaunay meshes*, Theoretical Computer Science, 296 (2003), pp. 145–165.

- [16] GARY L. MILLER, *A time efficient Delaunay refinement algorithm*, in Proceedings of the 15th annual ACM-SIAM symposium on Discrete algorithms, New Orleans, LA, 2004, pp. 400–409.
- [17] GARY L. MILLER, STEVEN E. PAV, AND NOEL WALKINGTON, *When and Why Ruppert's Algorithm Works*, in IMR, 2003, pp. 91–102.
- [18] GARY L. MILLER, DAFNA TALMOR, SHANG-HUA TENG, AND NOEL WALKINGTON, *A Delaunay based numerical method for three dimensions: Generation, formulation, and partition*, in Proceedings of the 27th Annual ACM Symposium on Theory of Computing, Las Vegas, NV, May 1995, pp. 683–692.
- [19] JIM RUPPERT, *A Delaunay refinement algorithm for quality 2-dimensional mesh generation*, Journal of Algorithms, 18(3) (1995), pp. 548–585.
- [20] JONATHAN RICHARD SHEWCHUK, *Constrained Delaunay tetrahedralizations and provably good boundary recovery*, in Eleventh International Meshing Roundtable, Ithaca, NY, Sept. 2002, pp. 193–204.
- [21] ———, *Delaunay refinement algorithms for triangular mesh generation*, Computational Geometry: Theory and Applications, 22 (2002), pp. 21–74.
- [22] ———, *What is a Good Linear Element? - Interpolation, Conditioning, and Quality Measures*, in Proceedings of the 11<sup>th</sup> International Meshing Roundtable, Sandia National Laboratories, September 2002, pp. 115–126.
- [23] ALPER ÜNGÖR, *Off-centers: A new type of Steiner points for computing size-optimal guaranteed-quality Delaunay triangulations*, in Proceedings of LATIN, Buenos Aires, Argentina, Apr. 2004, pp. 152–161.
- [24] DAVID F. WATSON, *Computing the n-dimensional Delaunay tessellation with application to Voronoi polytopes*, Computer Journal, 24 (1981), pp. 167–172.